

AD-A100 864

JAYCOR ALEXANDRIA VA  
STUDIES OF GYROTRON EFFICIENCY ENHANCEMENT AND CHERENKOV BROADB--ETC(U)  
AUG 80 R A SMITH, A DUDAS, J L VOMVORIDIS N00014-78-C-0613  
UNCLASSIFIED JAYCOR-PSD200-80-003-FR NL

1 of 1  
408 100064

END  
DATE  
FILED  
7-81  
DTC

AD A100364

01 0 30 011

LEVEL II

2

STUDIES OF GYROTRON EFFICIENCY  
ENHANCEMENT AND CHERENKOV BROADBAND  
AMPLIFICATION

APPROVED FOR PUBLIC RELEASE  
DISTRIBUTION UNLIMITED

JAYCOR Project 6101

JAYCOR Final Report No. PSD-200-80-003-FR  
Contract No. N00014-78-C-0613

August 5, 1980

DTIC  
SELECT  
S JUN 30 1981

Robert A. Smith

Alan Dudas

John L. Vomvoridis

JAYCOR  
205 S. Whiting Street  
Alexandria, VA 22304

Submitted to:

Office of Naval Research  
Arlington, VA. 22217

UNCLASSIFIED

**SECURITY CLASSIFICATION OF THIS PAGE (When Data Entered)**

REPORT DOCUMENTATION PAGE		READ INSTRUCTIONS BEFORE COMPLETING FORM	
1. REPORT NUMBER PSD200-80-003-FR ✓		2. GOVT ACCESSION NO. <i>AD-A100 864</i>	
4. TITLE (and Subtitle) Studies of Gyrotron Efficiency Enhancement and Cherenkov Broadband Amplification		5. TYPE OF REPORT & PERIOD COVERED Final Report 8/1/78 - 1/31/80	
7. AUTHOR(s) Robert A. Smith Alan Dudas John L. Nomvoridis		6. PERFORMING ORG. REPORT NUMBER - PSD200-80-003-FR	
9. PERFORMING ORGANIZATION NAME AND ADDRESS JAYCOR 205 S. Whiting St., Alex., VA 22304		10. PROGRAM ELEMENT, PROJECT, TASK AREA & WORK UNIT NUMBERS See attached sheet	
11. CONTROLLING OFFICE NAME AND ADDRESS Office of Naval Research Arlington, Virginia 22217		12. REPORT DATE 5 August 1980	
14. MONITORING AGENCY NAME & ADDRESS (if different from Controlling Office) Same as block 11		13. NUMBER OF PAGES 61	
16. DISTRIBUTION STATEMENT (for this Report) 1 copy - Scientific Officer 1 copy - Administrative Contracting Officer 6 copies - Director, NRL, Code 2627 12 copies - Defense Documentation Center 1 copy - ONR Branch Office - Pasadena		15. SECURITY CLASS. (of this report) UNCLASSIFIED 16. DECLASSIFICATION/DOWNGRADING SCHEDULE <i>APPROVED FOR PUBLIC RELEASE</i> <i>DISTRIBUTION UNLIMITED</i>	
17. DISTRIBUTION STATEMENT (for the abstract entered in Block 20, if different from Report) <i>75</i> <i>111-31</i> <i>117 24 10-1</i>			
18. SUPPLEMENTARY NOTES <i>Includes copy of NRL-MR-3983, ADA069461</i>			
19. KEY WORDS (Continue on reverse side if necessary and identify by block number)			
20. ABSTRACT (Continue on reverse side if necessary and identify by block number)			

## CONTENTS

	<u>Page</u>
I. DESIGN OF EXPERIMENT FOR TESTING EFFECTS OF TAPERED MAGNETIC FIELDS ON GYROTRON EFFICIENCY. . . . .	1
1. Introduction. . . . .	1
2. Design Considerations . . . . .	4
3. References. . . . .	9
II. ANALYSIS OF A BROADBAND CHERENKOV AMPLIFIER . . . . .	11
1. Introduction. . . . .	11
2. Analysis. . . . .	14
A. Physical Model. . . . .	14
B. Dispersion Relation . . . . .	15
3. Approximate Solution of the Dispersion Relation . .	19
APPENDIX - The Non-Linear Theory of Efficiency Enhance- ment in the Electron Cyclotron Maser . . . . .	33

Accession For	
NTIS GRA&I	<input checked="" type="checkbox"/>
DTIC TAB	<input type="checkbox"/>
Unannounced	<input type="checkbox"/>
Justification	
By	
Distribution/	
Availability Codes	
Dist	Avail and/or Special
A	

## PREFACE

The following tasks have been performed by JAYCOR under contract number N00014-78-C-0613:

A. The non-linear theory was developed for the efficiency enhancement of the electron cyclotron maser, by tapering the external magnetic field. This work has been published as NRL Memorandum Report 3983 by P. Sprangle and Robert A. Smith, and is presented in this report as an appendix.

B. The experimental design aspects have been considered for the effects of tapered magnetic fields on the gyrotron efficiency. This work is presented in Part I of this report.

C. An alternate configuration has been theoretically investigated, for the utilization of a Cherenkov-type interaction for the generation of radiation by an electron beam in a dielectrically loaded waveguide. This work is presented in Part II of this report.

## I. DESIGN OF EXPERIMENT FOR TESTING EFFECTS OF TAPERED MAGNETIC FIELDS ON GYROTRON EFFICIENCY

### 1. INTRODUCTION

The gyrotron has become a very promising source for high power mm wave radiation. To date with gyrotron oscillators (gyromonotrons) a power of 212 kW has been obtained on a CW basis at 28 GHz<sup>1</sup>, and 1 MW on a pulsed basis at 100 GHz.<sup>2</sup> Extrapolations to CW Megawatt operation at  $\geq$  100 GHz appears possible.<sup>3</sup> For the primary application presently foreseen for this type of device (electron cyclotron heating in magnetically confined fusion devices), efficiency will be of critical importance. Present devices appear to be limited to efficiencies of less than 50% even with the use of tapered cavity walls.<sup>1,2,4</sup> Recently methods have been proposed for increasing the efficiency to  $\sim$ 70%. These methods employ the varying of the magnetic field impressed on the cavity as a function of axial position. One method utilizes a step in the field,<sup>5</sup> the other a linear taper.<sup>6</sup> The methods are predicted to produce comparable efficiencies, but the latter appears to be more readily realized in practice.

A previous JAYCOR Report No. PSD200-80-002-FR discusses some aspects of the theory of efficiency enhancement due to external field nonuniformity. It explains the theory behind the trapping of beam particles as well as, qualitatively the significance of the various groups of particles being trapped. This is in an effort to explain the increased transfer of energy from the particles to the wave. Thus it provides background for the orbit integrator computer program developed by A. Drobot.

For the particular case of a linear magnetic taper in the direction of particle motion, extensive modeling and computer studies have been performed.<sup>6</sup> Parametric studies were performed using values determined by items already in house at NRL, (i.e., the Varian electron guns, power supplies, modulator, and superconducting magnets). The varied parameters consisted of: particle velocity ratio ( $\alpha^0 \equiv v_{10}/v_{z0}$ ); cavity length; mode numbers  $n, l$ ; wave field strength  $E_{\theta 0}$ ; uniform magnetic field strength  $B_0$ ; degree of linear magnetic tapering.

The initial experiment should be performed using a cavity with a length to radius ratio of 8. Since this is not one of the longer cavities the output power is expected to remain above 100 kW peak. Power output of the device scales roughly as  $\sim 1/L^3$  for the non-magnetically tapered device, and as  $\sim 1/L^{2.5}$  for the magnetically tapered gyrotron.<sup>3</sup>

From these studies, an optimum design was determined:

TE<sub>011</sub> mode

0.526 cm cavity wall radius

4.208 cm cavity length

35.0 GHz freq. of operation

14.8%  $\Delta B$  of magnetic taper

12.6 kG D.C. magnetic field value.

Since the product of  $Q \times P_{beam}$  is proportional to  $\omega \int E_{\theta}^2 2\pi r dr dl$  it is a measure of  $E_{\theta 0}^2$ . One of the outputs of the computer code is the value of this product at the point of optimum efficiency. The computed value for the experiment described above is  $Q_{beam}^{opt} = 126$  MW for an electronic efficiency of approximately 49% with magnetic tapering. The predicted efficiency without tapering is only computed to be ~33.5%.

The minimum, or diffraction  $Q^7$  of this cavity is approximately given by the formula  $\frac{4\pi}{\lambda}(L/\lambda_0)^2$ , which for this case is  $\sim 300$ . It is expected that an experimentally feasible  $Q$  will be in the range of  $2Q_{\text{diff}}$ .

Two different methods for tapering the magnetic field should be utilized, depending on the length of the experimental cavity and the amount of tapering necessary. The first method is to position a shaped steel piece around the cavity to act as a flux gatherer. This, of course, allows no way of actively varying the amount of tapering other than replacing the steel cones. The second method consists of a coil wound around the external surface of the gyrotron in the cavity region. The advantage of this over the steel cone is that the current through the coil could be varied to produce the exact amount of tapering to optimize the efficiencies for certain operating conditions. For high degrees of tapering heating of the coil windings may become a problem; pulsing the coil may be required.

## 2. DESIGN CONSIDERATIONS

The mechanical design of the device is shown in Figure 1. The design permits rapid exchange of the cavity, output loading, and input beam guide sections, in that these parts can be inserted from the electron gun end of the tube without the breaking of welds. We note that the components are positioned together only by slight pressure from the end flange gasket - a method feasible only because the electromagnetic mode of operation,  $TE_{01}$ , requires no axial currents.

### (a) Electron Gun.

The electron accelerator is of NRL/Varian design<sup>8,9</sup>, and manufactured by Varian. The design calls for an operating voltage of 70 kv, with a beam current of 8-10A. Under these conditions, the ratio of perpendicular to parallel electron velocities should be 1.5, and the spread in the parallel and perpendicular velocities should be 10% and 7%, respectively. Estimates indicate that these spreads should not significantly affect the maser mechanism.<sup>10</sup>

### (b) Beam Input Guide.

For initial experimentation the input guide used should be very similar to that used in the initial gyrotron. This has an I.D. near the gun of 1.067 cm and tapers toward the cavity to .940 cm. It is slotted with azimuthal slots to help prevent axial wall currents, and is backed by poco graphite as an absorber.

There is some question as to whether at higher beam currents there may be some beam interception or even some type of oscillation occurring in the beam guide. Should this occur a second type of beam input guide might be employed. This could consist of alternating discs of copper rings and type 2710 Ceralloy, a microwave absorber.

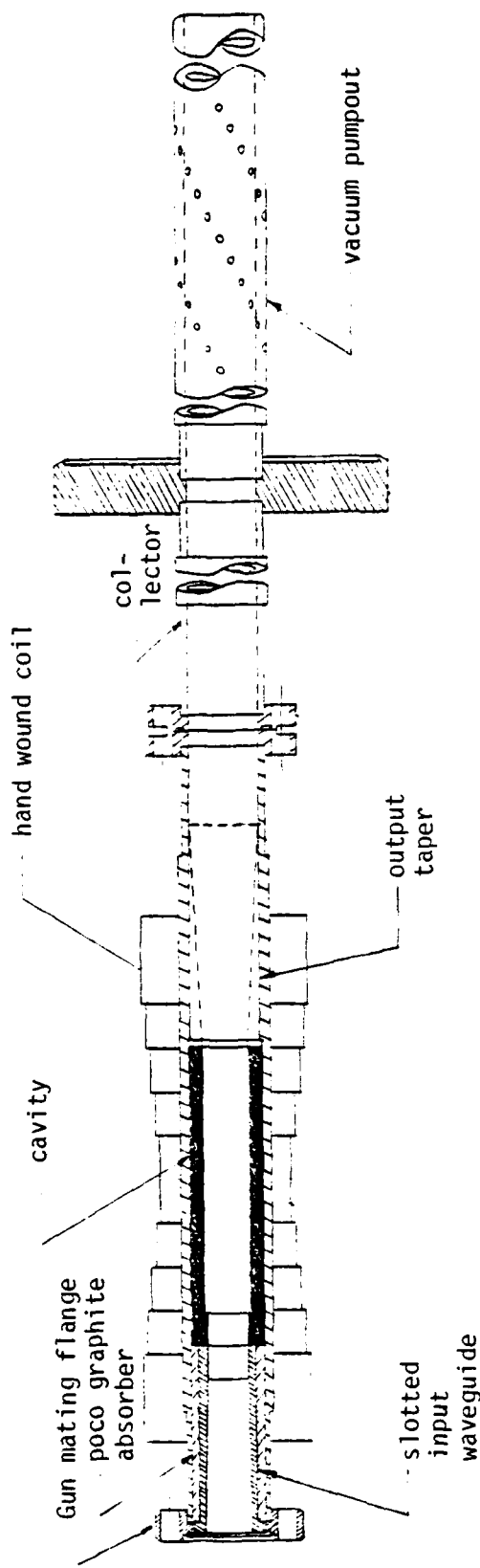


Figure 1

In order to thoroughly study the impact of magnetic tapering, several different length cavities should be used during the course of the experimentation. It is desirable that the cavity be centered on the magnetic taper such that the center of the cavity corresponds to a point in the tapered magnetic field equivalent to the D.C. magnetic field value. To accommodate the different length cavities, spacers should be designed to maintain the proper cavity-field alignment.

(c) Output Waveguide and Collector.

The output guide was chosen to be a standard circular waveguide size, with a diameter of 1.603 cm. This guide has approximately fifty 0.159 cm diameter holes drilled in it for pumping. It also serves as a rudimentary collector allowing pulse rates of  $\sim 10$  pps.

(d) Output Window.

The output window used on the tapered magnetic field gyrotron should be a one half wave length resonant window fabricated from beryllia (Figure 2). The window is of the same diameter as the 1.603 cm waveguide.<sup>4</sup> Thus the entire device from the output waveguide to the mode converted will be of uniform diameter. Test results for this window are shown in Figure 3.

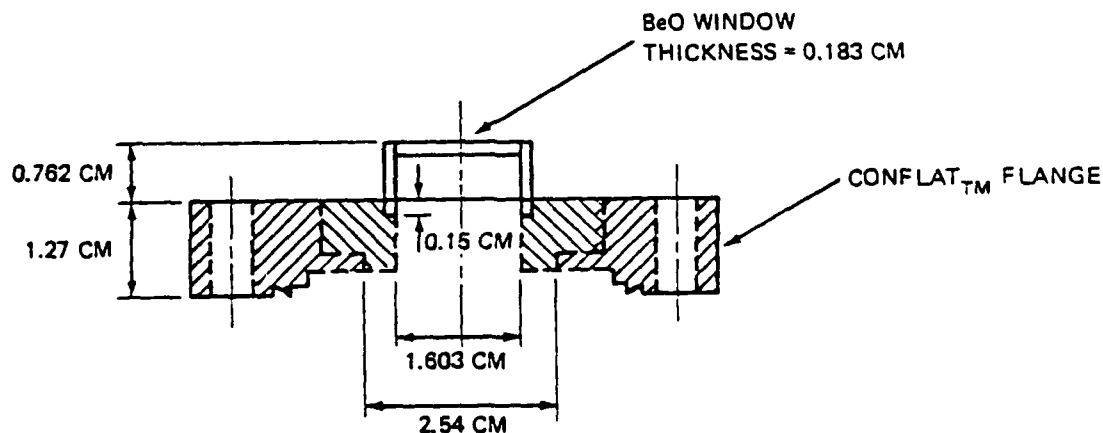


Figure 2

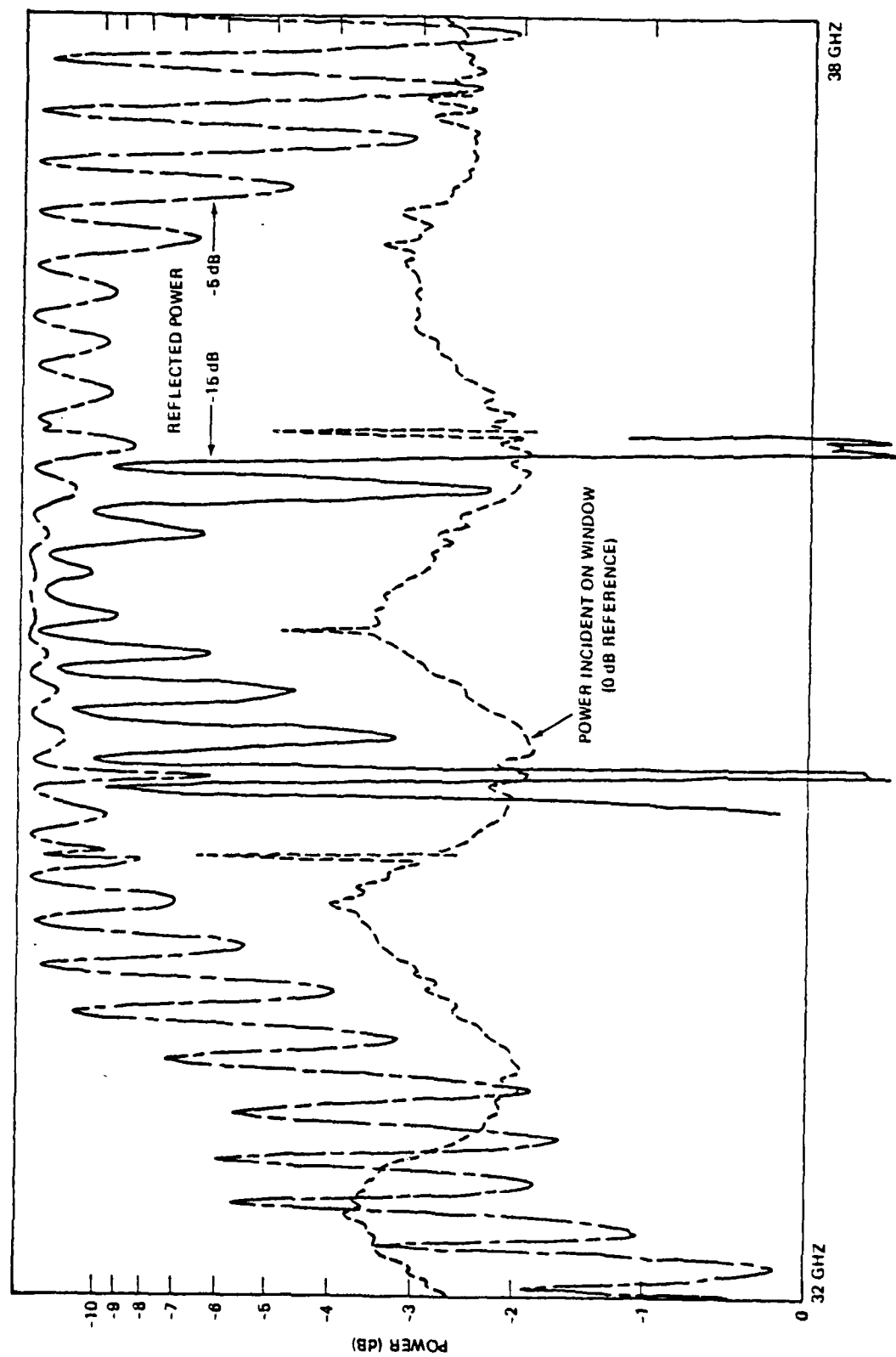


Figure 3. Plot of incident and reflected power versus frequency for the small window. The window was tested in place in the output waveguide.

(e) Converter and Filter.

The gyrotron discussed in this report was designed to produce radiation in the  $TE_{01}$  (circular) mode. This mode, while being very low loss, cannot be focused and is difficult to handle. It is therefore desirable to convert the radiation into a rectangular mode, ( $TE_{10}$ ) which can be focused and can be handled using readily available components. The converter chosen was made by Hitachi Corporation and has been used on the previous model gyrotron. A mode filter which absorbs all non  $TE_0^0$  modes will be used to reduce reflections.

### 3. REFERENCES

1. Microwave Journal, "Microwave Power Tube Conference Report", Vol. 23, No. 7, July 1980.
2. A. V. Gaponov, et. al., "Some Perspectives of the use of Powerful Gyrotrons for the Electron-Cyclotron Plasma Heating in Large Tokamaks", Report for IV International Conference on Infrared and Nearmillimeter Waves, December 1979.
3. M. E. Read, K. R. Chu, K. J. Kim, "Power Limits in Cylindrical Gyromonotrons Using  $TE_{0n}$  Modes." (To be published).
4. M. E. Read, K. R. Chu, V. L. Granatstein, R. M. Gilgenbach, R. Lucey, Jr., A. T. Drobot, "Spatial and Temporal Coherence of a 35 GHz Gyromonotron Using the  $TE_{01}$  Circular Mode." (To be published in IEEE-MTT).
5. P. Sprangle, R. A. Smtih, K. R. Chu, "The Non-Linear Theory of Efficiency Enhancement in the Electron Cyclotron Maser", NRL Memo Report #3983.
6. K. R. Chu, M. E. Read, A. K. Ganguly, "Methods of Efficiency Enhancement and Scaling for the Gyrotron Oscillator, NRL Memorandum.
7. "Study on the Initial Development of High-Power Millimeter Wave Sources" JAYCOR Project #2061.
8. J. L. Seftor, K. R. Chu, and A. T. Drobot, "An Investigation of a Magnetron Injection Gun Suitable for Use in Cyclotron Resonance Masers," NRL Memo Report 3697, (1978).
9. Varian Associates, "Technical Report on the Design of an Electron Gun for a Cyclotron Resonance Maser," under NRL Contract N00173-77-C-0086, (June 1967).

10. K. R. Chu, "Theory of Electron Cyclotron Maser Interactions in a Cavity at the Harmonic Frequencies", NRL Memo Report 3672, (1977).

## II. ANALYSIS OF A BROADBAND CHERENKOV AMPLIFIER

### 1. INTRODUCTION

In the past several years, there has been widespread interest in a variety of wave generation devices based on un-neutralized beams of relativistic or mildly relativistic electrons. Such devices are potentially capable of producing high power, with high efficiency, in the centimeter, millimeter, and sub-millimeter spectral ranges. An example is the electron cyclotron maser, which has produced  $\approx 100$  kW at centimeter wavelengths, with efficiencies ranging from 30% - 50%. The gyrotron mechanism involves azimuthal phase bunching of the electron beam, which occurs during resonant interaction of the Doppler-shifted beam cyclotron mode with a waveguide or cavity mode (Fig. 1). The bandwidth of the gyrotron mechanism is typically of order 1-2%.

For various military and communications applications, it could be of great interest to develop free-electron amplifiers with wide operating bandwidths  $\Delta\omega \gtrsim \omega$ . In this report, we present a linear analysis of a new principle for wideband amplification. The basic configuration is the use of an annular electron beam drifting in a dielectrically-loaded waveguide (Fig. 2). In such a waveguide, the normal guide modes have phase velocities asymptotic to  $c\sqrt{\epsilon}$ , where  $c$  is the speed of light and  $\epsilon > 1$  is the dielectric constant (assumed to be isotropic) of the waveguide lining. The system is assumed to be immersed in an axial magnetic field,  $B_0$ , sufficiently strong to render the motion of the beam electrons one-dimensional. In this case,

the amplification mechanism depends on axial charge bunching in the Cerenkov interaction of a longitudinal space-charge wave of the beam with the  $E_z$  - component of a TM guide mode.

The interaction we envision is schematically represented in the dispersion diagrams of Fig. 3, where

$$\omega_{\pm} = kV \pm \frac{\omega_p}{\sqrt{\epsilon\gamma^3}} \quad (1)$$

are the positive and negative energy beam modes and

$$\omega_g = \pm \frac{1}{\epsilon} \sqrt{(kc)^2 + \left(\frac{2.4c}{r_4}\right)^2} \quad (2)$$

are the waveguide modes for the case of a constant isotropic dielectric material filling the waveguide. As can be seen in Fig. 3a, where  $\epsilon=1$ , the beam and guide modes do not cross and therefore four distinct propagating modes are expected on the entire  $k$  spectrum, with their dispersion characteristics given by slight modification of Eqs (1) and (2) due to coupling. On the other hand however, Fig. 3b, when  $\epsilon \neq 1$  and in particular when  $\epsilon > (c/V)^2$  the dispersion curves do cross and therefore growing modes are expected due to the interaction. Most interesting appears to be the case when  $\epsilon$  slightly exceeds the value  $(c/V)^2$ , since then strong interaction is expected over a broad band of frequencies.

The above discussion applies also to the topologically equivalent

case of a waveguide with partial dielectric filling, for which the dispersion curve is represented by the broken line in Fig. 3b. Since this configuration is more compatible with  $\epsilon \gtrsim (c/v)^2$ , the analysis of this report is based on the realistic geometry of Fig. 2.

In Section 2, we present the general linear analysis of this system, culminating in the dispersion relation of Eq.(11). In Section 3, the dispersion relation is solved analytically in a simple limiting case. In Section IV, we present the conclusions of this analysis and suggestions for future work on this concept.

## 2. ANALYSIS

### A. Physical Model

The configuration and geometrical parameters are defined in Figure 2. The waveguide is a perfectly conducting cylinder of radius  $r_4$ . The guide is lined with a lossless dielectric (of isotropic dielectric constant  $\epsilon$ ) in the space  $r_3 \leq r \leq r_4$ . The electron beam is annular, filling the region  $r_1 \leq r \leq r_2$ . The regions  $0 \leq r < r_1$ ,  $r_2 \leq r \leq r_3$  are in vacuum. An applied axial magnetic field  $B_0 = B_0 \hat{e}_z$  pervades the waveguide. The un-neutralized electron beam has purely axial motion; this corresponds to the limit  $B_0 \rightarrow \infty$ , so that transverse motion is suppressed and no cyclotron interaction may occur. We assume a cold uniform annular beam, the equilibrium distribution function of which is given by

$$f_0(r, p_z) = n_0 H(r - r_1) H(r_2 - r) \delta(p_z - \gamma_0 m V) \quad (3)$$

where  $\gamma_0 = (1 - V^2)^{-1/2}$  and  $H(x)$  is the Heaviside step function, and where  $\omega_b^2 = 4\pi n_0 e^2 \int \gamma_0 m$ .

As discussed in the introduction, when  $V > c/\sqrt{\epsilon}$  so that the unperturbed beam and guide modes intersect, we expect instability (Fig. 4).

### B. Dispersion Relation

We seek to derive the general dispersion relation for this instability, in order to obtain quantitative results for the parameters of interest for the design and operation of a device to act as a broad-band amplifier. Such parameters, indicated in Fig. 4, are:

- The optimal frequency,  $\omega_m$ , for which the amplification rate is largest.
- The corresponding spatial growth rate,  $\delta k_I$ .
- The cutoff frequency,  $\omega_0$ , corresponding to the modified waveguide curve.
- The upper cutoff frequency,  $\omega_1$ , of the unstable range
- The choice of values for  $\epsilon$ ,  $V$ ,  $n$  etc for which  $\omega_1 - \omega_m$  and/or  $\delta k_I$  maximize.

To derive the dispersion relation for the coupled beam-guide system of Figure 2, we consider  $TM_{00,k}$  modes (i.e., no azimuthal dependence).

The wave fields are given by

$$\vec{E}(r, z, \theta, t) = [E_z(r) \hat{e}_z + E_r(r) \hat{e}_r] e^{ikz - i\omega t}, \quad (4)$$

$$\vec{B}(r, z, \theta, t) = B_\theta(r) \hat{e}_\theta e^{ikz - i\omega t}, \quad (5)$$

where  $E_z(r)$  is the solution of the wave equation

$$\left\{ \frac{1}{r} \frac{d}{dr} \left( r \frac{d}{dr} \right) - \left[ k^2 - \epsilon(r) \frac{\omega^2}{c^2} \right] h^2(\omega, k, r) \right\} E_z(r) = 0, \quad (6)$$

with  $E_r$  and  $B_\theta$  given by:

$$E_r(r) = \frac{ik}{\epsilon(r) \omega^2/c^2 - k^2} \frac{d}{dr} E_z(r) , \quad (7)$$

$$H_\theta = \frac{\omega}{ck} D_r , \quad (8)$$

and  $D_r = \epsilon E_r$ ,  $H_\theta = B_\theta/\mu$ , with  $\mu$  being the magnetic permittivity.

The quantity  $h^2(\omega, k, r)$  is the plasma dielectric function

$$h^2(\omega, u, r) = 1 - \frac{4\pi e^2}{m \epsilon(r)} \int \frac{dp_z f_0(v, p_z)}{\gamma^3 (\omega - kv_z)^2} , \quad (9)$$

where the equilibrium distribution function  $f_0(r, p_z)$  given by Eq.3 will be assumed.

Using Eqs. (4) - (9), the dispersion relation is obtained by applying the boundary conditions:

$$\begin{aligned} E_z(r_4) &= 0 , \\ [E_z(r)] &= [B_\theta(r)] = 0 \quad (r = r_1, r_2, r_3) , \end{aligned} \quad (10)$$

where  $[\psi(r)]$  indicates the jump in quantity  $\psi(r)$  across the interface at  $r$ . The seven conditions (10) yield the dispersion relation.

$$\begin{bmatrix}
- I_0(k_0 r_1) & I_0(k_0 h r_1) & K_0(k_0 h r_1) & 0 & 0 & 0 \\
- I_1(k_0 r_1) & h I_1(k_0 h r_1) & - h K_1(k_0 h r_1) & 0 & 0 & 0 \\
0 & I_0(k_0 h r_2) & K_0(k_0 h r_2) & - I_0(k_0 r_2) & - K_0(k_0 r_2) & 0 \\
0 & h I_1(k_0 h r_2) & h K_1(k_0 h r_2) & - I_1(k_0 r_2) & K_1(k_0 r_2) & 0 \\
0 & 0 & 0 & - I_0(k_0 r_3) & - K_0(k_0 r_3) & J_0(k_E r_3) \\
0 & 0 & 0 & - k_E I_1(k_0 r_3) & k_E K_1(k_0 r_3) & \varepsilon k_0 J_1(k_E r_3) \\
0 & 0 & 0 & 0 & 0 & J_0(k_E r_4) \\
0 & 0 & 0 & 0 & 0 & Y_0(k_E r_4)
\end{bmatrix}$$

where

$$k_0^2 = k^2 - \omega^2/c^2 , \quad (12a)$$

$$k_E^2 = \epsilon \omega^2/c^2 - k^2 , \quad (12b)$$

$$h^2 = 1 - \frac{1}{\gamma_0^3} \left( \frac{\omega_b}{\omega - kv_0} \right)^2 , \quad (12c)$$

the last expression being the dielectric for a cold beam,  $f_0 \sim \delta(p_z - p_0)$  and where  $J_m$ ,  $Y_m$  ( $I_m$ ,  $K_m$ ) are the ordinary (modified) Bessel functions of order  $m$ . Equation (11) is the central result of the analysis. It must be solved numerically, giving the wavenumber ( $\text{Re } k$ ) and spatial growth rate ( $-\text{Im } k$ ) for real  $\omega$ .

3. APPROXIMATE SOLUTION OF THE DISPERSION RELATION

An approximate analytic solution of Eq. (11) can be obtained in the limit where we consider a thin annular beam at the dielectric interface; i.e.,

$$r_3 - r_2 \rightarrow 0; \quad r_{21} \equiv r_2 - r_1 \ll r_1. \quad (13)$$

The introduction of this limit is done not just for the sake of the simplification and tractability it introduces to the equations, but also because it corresponds to that of the most efficient operation. In fact, since the waveguide modes outside the dielectric material are proportional to the modified Bessel function, their amplitude is maximum near the dielectric interface, hence, it is desirable to place the beam the closest possible to the dielectric to maximize the coupling coefficient.

Under these assumptions, Eq. (11) can be simplified to yield the dispersion relation

$$\frac{1}{k_0} - \frac{I_1(k_0 r_2)}{I_0(k_0 r_2)} - \epsilon \frac{1}{k_E} \left[ \frac{J_1(k_E r_2) Y_0(k_E r_4) - Y_1(k_E r_2) J_0(k_E r_4)}{J_0(k_E r_2) Y_0(k_E r_4) - Y_0(k_E r_2) J_0(k_E r_4)} \right] + r_{21} h^2 = 0. \quad (14)$$

From Eq. (14), we may extract several limiting cases:

(a) If either  $k_E r_2 \gg 1$  or  $k_E r_{42} \equiv k_E(r_4 - r_2) \ll 1$ , we have

$$\frac{J_1(k_E r_2) Y_0(k_E r_4) - Y_1(k_E r_2) J_0(k_E r_4)}{J_0(k_E r_2) Y_0(k_E r_4) - Y_0(k_E r_2) J_0(k_E r_4)} \approx \operatorname{ctn}(k_E r_{42}) , \quad (15)$$

giving

$$\frac{1}{k_0} \frac{I_1(k_0 r_2)}{I_0(k_0 r_2)} - \frac{\epsilon}{k_E} \operatorname{ctn}(k_E r_{42}) + r_{21} h^2 = 0 . \quad (16)$$

(b) If  $k_0 r_2 \gg 1$ , then

$$\frac{I_1(k_0 r_2)}{I_0(k_0 r_2)} \approx 1 - \frac{1}{2 k_0 r_2} \approx 1 , \quad (17)$$

giving

$$\frac{1}{k_0} - \frac{\epsilon}{k_E} \operatorname{ctn}(k_E r_{42}) + r_{21} h^2 = 0 \quad (18)$$

Equation (17) is not valid near the cutoff  $\omega_0$ . The result (18) is identical to that obtained in planar geometry; this is the limiting case of large aspect ratio.

(c) Near the beam modes,  $k_E r_{42} \lesssim \pi/2$ , and we have

$$\frac{1}{k_0} - \frac{\pi}{2} \frac{\epsilon}{k_E} + \epsilon r_{42} = - r_{21} h^2 . \quad (19)$$

The cutoff frequency  $\omega_0$  ( $k = 0$ ) is obtained from

$$\frac{J_1(\omega_0 r_2/c)}{J_0(\omega_0 r_2/c)} = \epsilon^{\frac{1}{2}} \operatorname{ctn} \left( \frac{\omega_0 r_2}{c} \frac{\epsilon^{\frac{1}{2}} r_{42}}{r_2} \right) \quad (20)$$

For  $\epsilon^{\frac{1}{2}} r_{42} \gg r_2$ , implying  $\omega_0 r_2/c < 1$ , we find

$$\omega_0 = \frac{\pi c}{2\epsilon^{\frac{1}{2}} r_{42}} \left( 1 + \frac{r_2}{2\epsilon r_{42}} \right)^{-1} = \frac{\pi c}{2\epsilon^{\frac{1}{2}} r_{42}} \quad (21)$$

For  $\epsilon^{\frac{1}{2}} r_{42} \lesssim r_2$  ( $\omega_0 r_2/c \gtrsim 1$ ), we have

$$\omega_0 = 2.405 c/r_4 \quad (22)$$

Near the beam mode, we have from Eq. (19) the form

$$(\omega - kc\beta)^2 \left[ \frac{1}{k_0(\omega, k)} - \frac{\pi}{2} \frac{\epsilon}{k_E(\omega, k)} + \epsilon r_{42} \right] = r_{21} \frac{\omega_b^2}{\gamma_0^3} \quad (23)$$

where  $\beta \equiv V_0/c$ .

Taking  $k = \omega/\beta c + \delta k$ , where  $|\delta k| \ll |k|$ ,

we find

$$(\delta k)^2 D_g(\omega, k) = \frac{r_{21} \omega_b^2}{\gamma^3 \beta^2 c^2} \quad (24)$$

where

$$D_g(\omega, k) = \frac{1}{k_0} - \frac{\pi}{2} \frac{\epsilon}{k_E} + \epsilon r_{42} \quad (25)$$

Expanding  $D_g$  about  $k = \omega/\beta c$ , we have

$$(\delta k)^2 \left[ D_g(\omega, \frac{\omega}{\beta c}) + \frac{\partial D_g}{\partial k}(\omega, \frac{\omega}{\beta c}) \delta k \right] = \frac{r_{21}\omega^2}{\gamma^3 \beta^2 c^2} , \quad (26)$$

which can be solved for  $\delta k(\omega)$ . The maximum growth rate is obtained at  $\omega \equiv \omega_m$  for  $D_g(\omega_m, \omega_m/\beta c) = 0$ , giving

$$\omega_m = \frac{\pi}{2} \frac{c}{r_{42}} \frac{\beta}{\sqrt{\epsilon \beta^2 - 1}} \left[ 1 - \frac{2}{\pi} \frac{\gamma}{\epsilon} \sqrt{\epsilon \beta^2 - 1} \right] \quad (27)$$

as the frequency at which the growth rate maximizes; the corresponding growth rate is given by the imaginary part of  $\delta k_m$ , where,

$$\delta k_m^3 = - \frac{r_{21}\omega_p^2}{r_{42}^2 c^2} \frac{\pi}{2} \frac{\sqrt{\epsilon \beta^2 - 1}}{\epsilon \beta^2 \gamma^3} \frac{\left[ 1 - \frac{2}{\pi} \frac{\gamma}{\epsilon} \sqrt{\epsilon \beta^2 - 1} \right]^2}{\left[ 1 + \frac{2}{\pi} \frac{\gamma^3}{\epsilon} (\epsilon \beta^2 - 1)^{3/2} \right]} \quad (28)$$

From Eqs. (27) and (28) we deduce an important constraint, viz, that the spatial growth rate and frequency bandwidth are universally related. Large growth rates can be obtained at the expense of limited bandwidth, and vice versa. To see this, we note that  $|(\delta k_m)^3|$  maximize for

$$\epsilon \gg 1; \epsilon \beta^2 \rightarrow 2 , \quad (29)$$

where we set  $\gamma \sim 1$  (i.e., the beam is only weakly relativistic). In this limit, we find

$$\omega_m = \frac{\pi c}{2r_{42}} \frac{\beta}{\sqrt{\epsilon \beta^2 - 1}} , \quad (30)$$

and

$$(\delta k)_m = \frac{1}{2} \left(1 - i\sqrt{3}\right) \frac{1}{\gamma} \left[ \frac{r_{21}\omega_b^2}{r_{42}^2 c^2} \frac{\pi}{2} \frac{(\epsilon\beta^2 - 1)^{1/2}}{\epsilon\beta^2} \right]^{1/3} . \quad (31)$$

Thus in the limit  $\epsilon^{1/2} r_{42} > r_2$  (for  $\epsilon \gg 1$ ), we have

$$\frac{\omega_{on}}{\omega_0} = \sqrt{\frac{\epsilon\beta^2}{\epsilon\beta^2 - 1}} = \sqrt{2} \quad (32)$$

under the conditions (29) for which  $|\delta k_m|$  is maximum.

On the other hand, the bandwidth  $\delta\omega$  is given by the upper cutoff frequency  $\omega_1$ , where  $\text{Im}\delta k = 0$ , as

$$\delta\omega = \omega_1 - \omega_m = \frac{3}{2\gamma} \left[ \frac{cr_{21}\omega_b^2}{r_{42}^2} \frac{\pi\beta}{\epsilon} (\epsilon\beta^2 - 1)^{-5/2} \right]^{1/3} \quad (33)$$

Thus from (28) and (33) we find the very useful relation

$$\frac{\delta\omega}{c\text{Im}\delta k_m} = 2.18 \frac{\beta}{\epsilon\beta^2 - 1} , \quad (34)$$

which yields a maximum for  $\delta\omega$  at

$$\epsilon \rightarrow 2, \quad \epsilon\beta^2 \rightarrow 1, \quad \gamma \rightarrow \sqrt{2} ; \quad (35)$$

the regime (35) is seen to be the opposite limit to that of relation (29).

We shall briefly discuss the consequences of relaxing a simplifying assumption we have used in the analysis, viz that the beam is taken to be cold and uniform in density. We have neglected effects of temperature and energy shear. Across the beam, the wave field is given approximately (for  $r_{21} \ll r_1$ ) by

$$\left[ \frac{d^2}{dr^2} - k_0^2 h^2(r) \right] E_z(r) = 0 , \quad (36)$$

where

$$h^2(r) = 1 - \frac{4\pi e^2}{m} \int \frac{f_0(r, p) dp}{\gamma^3(\omega - kv)^3} \quad (37)$$

If  $h(r)$  is a smooth function, Eq. (36) has the WKB solution

$$E_z(r) = h^{-\frac{1}{2}} \exp \left( k_0 \int h(r) dr \right) . \quad (38)$$

We may estimate the effects of energy spread and self fields (manifested in the potential  $\phi(r)$ ), by taking an equilibrium distribution of the form

$$f_0(r, p) = \frac{1}{\sqrt{\pi m} E_{th}} \sqrt{\frac{p^2}{2m} - e\phi(r)} \exp \left[ - \frac{(p^2/2m - e\phi(r) - E_0)^2}{2 E_{th}^2} \right] , \quad (39)$$

where  $E_0$  is the nominal beam energy and  $E_{th}$  is a measure of thermal energy spread. Then the quantity  $\omega_b^2/\gamma^3(\omega - kv)^2$  used for the analysis of a cold beam is to be replaced by

$$\frac{\omega_{p0}^2}{\gamma_0^3 (\omega - kv_0)^3} \left\{ 1 - \sqrt{\frac{2}{mE_0}} \frac{ek\delta\phi}{\omega_{bo}} + \frac{3k^2}{2m(E_0 + e\phi_0)} \frac{E_{th} + e^2\delta\phi^2}{\omega_{bo}^2} \right\} \quad (40)$$

where quantities subscripted "zero" are evaluated at the center of the beam and where

$$e\delta\phi = m\omega_{bo}^2 r_{21}^2/8 \quad (41)$$

is the potential energy drop between the edge and the center of the beam. The energy shear associated with the self-fields has two effects:

(i) The effective beam density  $\omega_{bo}^2$  is reduced:

$$\omega_{bo}^2 \rightarrow \omega_{bo}^2 \left( 1 - \frac{ek\delta\phi}{\sqrt{2mE_0}\omega_b} \right)^2 ; \quad (42)$$

(ii) The effective energy spread is increased:

$$E_{th} \rightarrow \left[ E_{th}^2 + \frac{2}{3} e^2 \delta\phi^2 \right]^{\frac{1}{2}} . \quad (43)$$

Summary

In the analysis of Sections 2 and 3 we have demonstrated the validity of the dielectric-loaded Cerenkov wide-band amplifier concept. We have obtained approximate relations for the growth rate and bandwidth, revealing an important tradeoff between them, cf. Eq. (34), which must be considered in design applications.

An important extension of this work would be to consider a nonlinear calculation in order to elucidate the saturation mechanism (which we expect to be beam trapping) and ultimate power levels.

FIGURE CAPTIONS

Figure 1 - Dispersion curves for the waveguide mode and the electron cyclotron mode in the electron cyclotron maser.

Figure 2 - Geometry of the Broadband Amplifier.

Figure 3a- Dispersion curves for the waveguide mode and the beam modes when  $\epsilon = 1$ .

Figure 3b - Dispersion curves for the waveguide mode and the beam modes when the waveguide is filled with a dielectric material with  $\epsilon > (c/V)^2$ . The broken curve refers to a partially filled waveguide.

Figure 4 - Wavenumber,  $\text{Re}(k)$ , and spatial growth rate,  $\text{Im}(k)$  for the instability (schematically). The solid curves indicate the unamplified propagating modes.

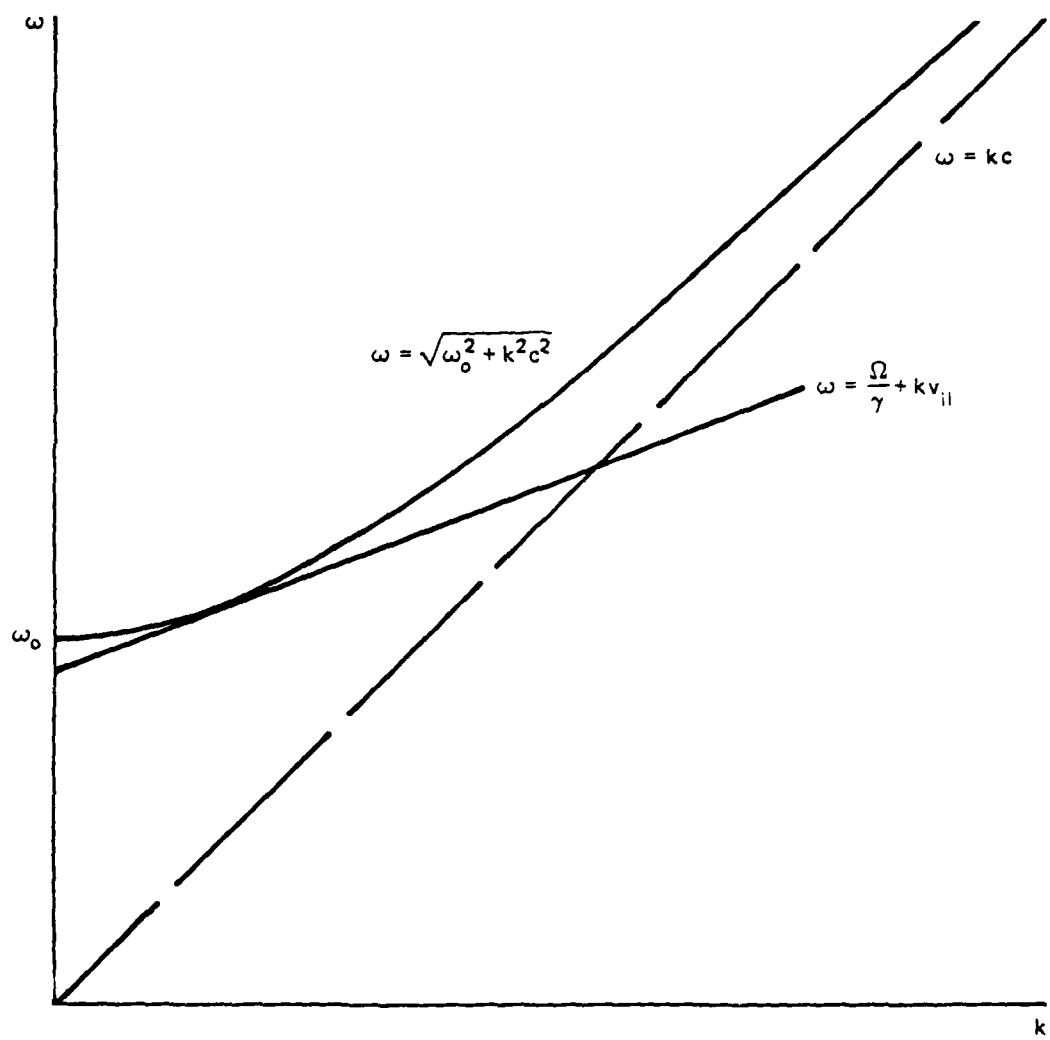


Figure 1

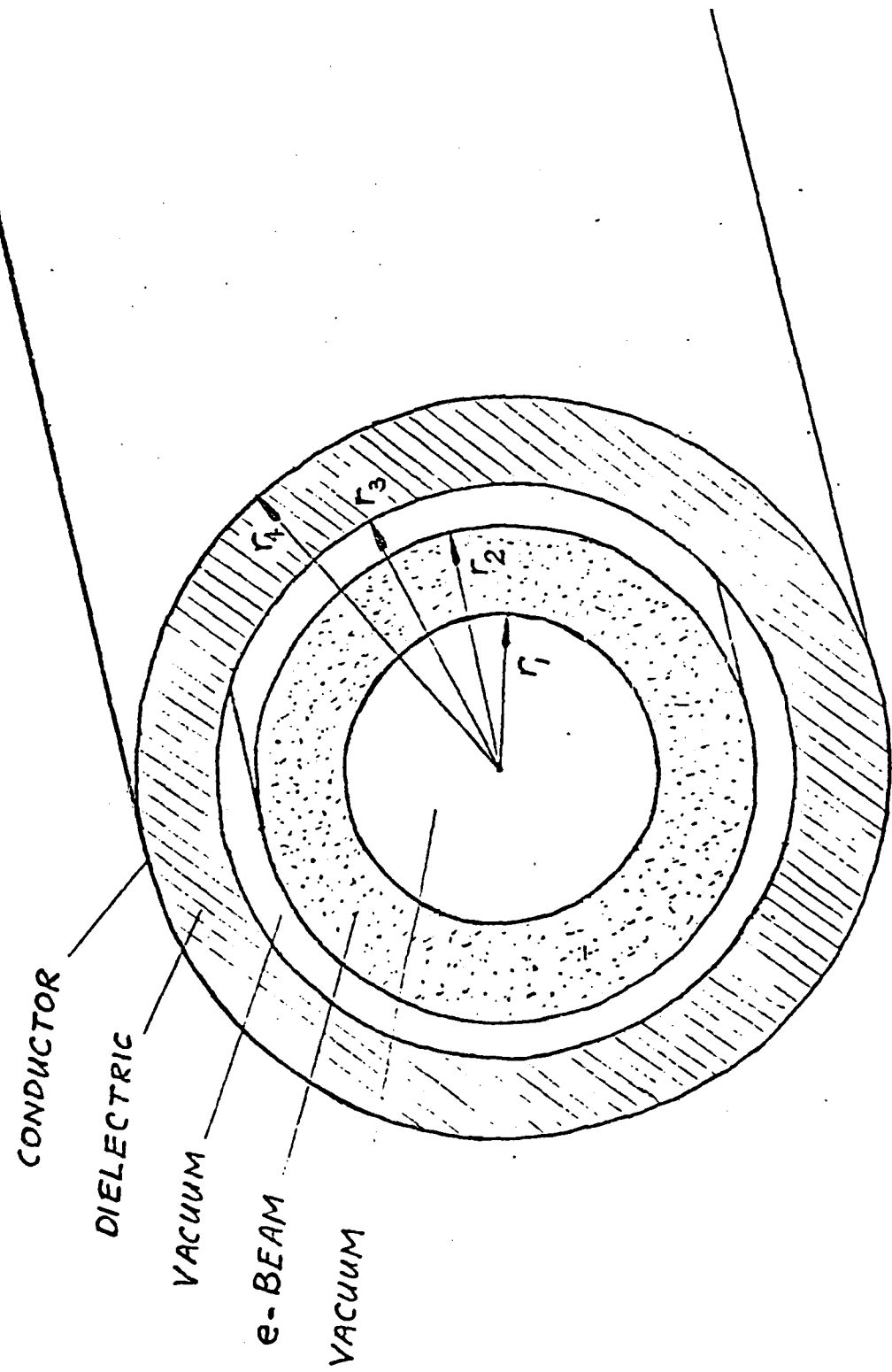


Figure 2

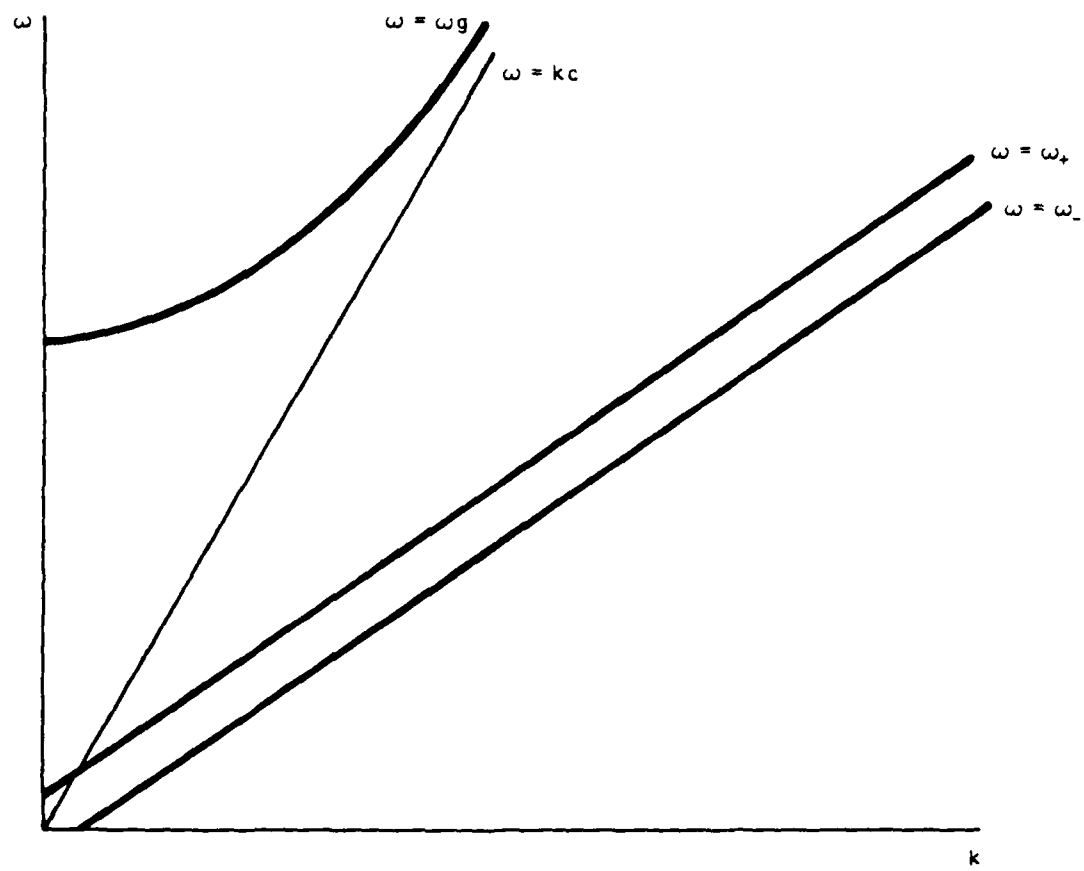


Figure 3a

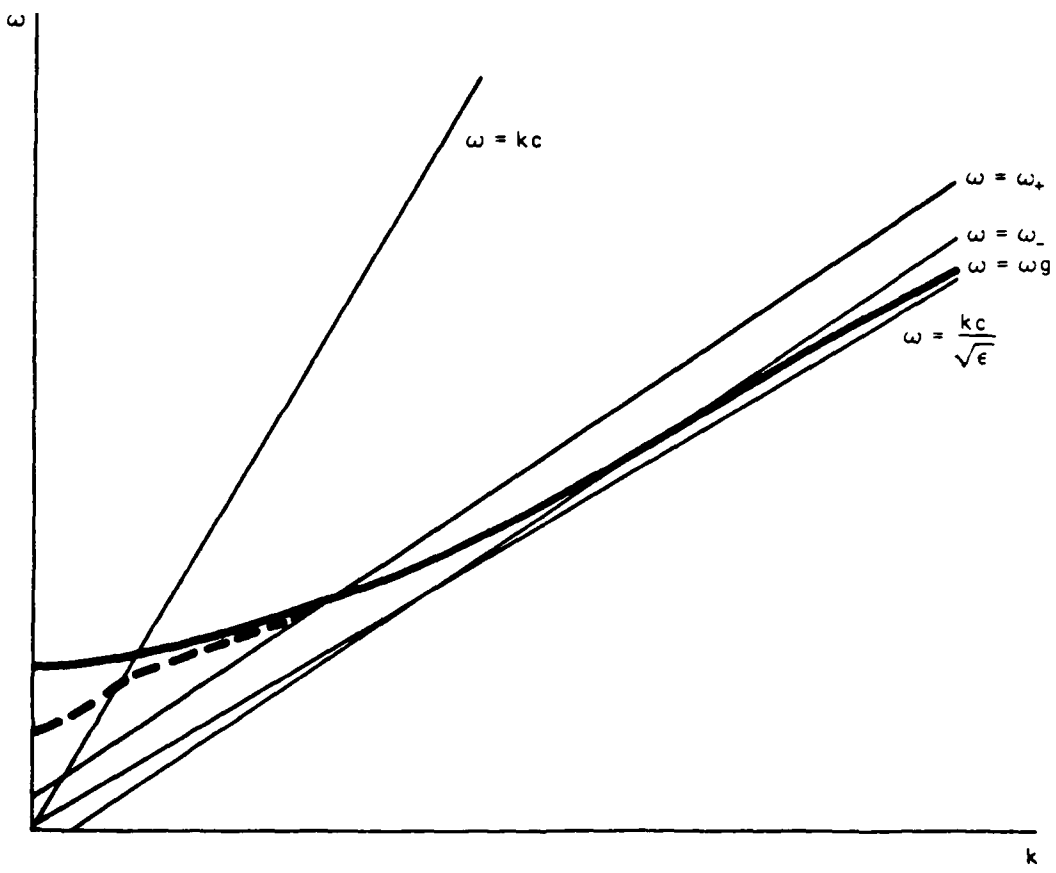


Figure 3b

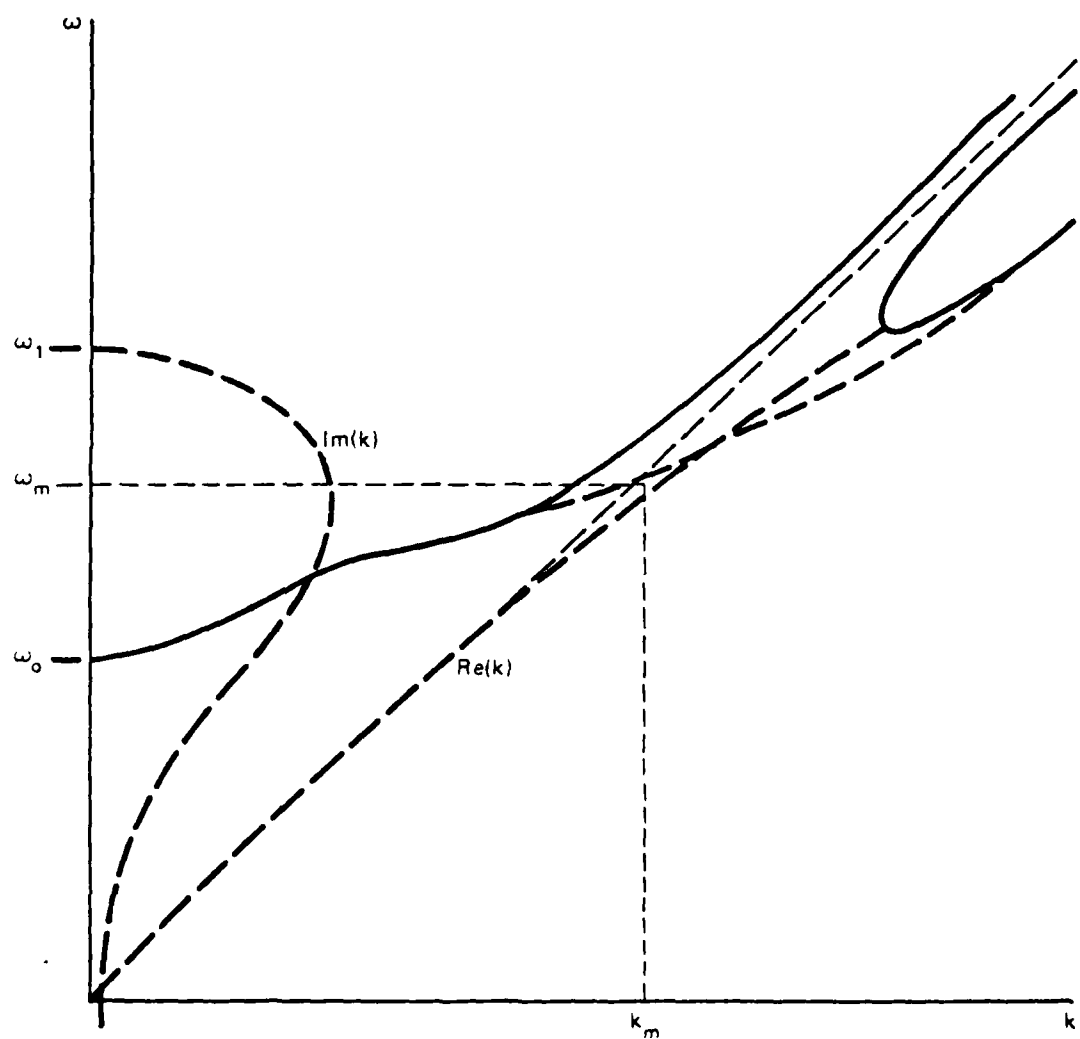


Figure 4

APPENDIX

THE NON-LINEAR THEORY OF EFFICIENCY ENHANCEMENT  
IN THE ELECTRON CYCLOTRON MASER

## CONTENTS

I. INTRODUCTION .....	1
II. ANALYSIS .....	3
a. Maser Cavity Model .....	3
b. Particle Dynamics .....	3
c. Forward or Backward Wave Coupling .....	5
III. ENHANCEMENT OF MASER EFFICIENCY .....	8
IV. CONCLUSION .....	11
ACKNOWLEDGMENTS .....	11
REFERENCES .....	12

## THE NON-LINEAR THEORY OF EFFICIENCY ENHANCEMENT IN THE ELECTRON CYCLOTRON MASER

### I. INTRODUCTION

Radiation sources based on the electron cyclotron maser mechanism are perhaps the most efficient devices for generating high continuous power in the millimeter and submillimeter regimes. The first theoretical work<sup>1-3</sup> on the cyclotron maser mechanism showed the relativistic nature of the instability while experimental confirmation came shortly afterwards.<sup>4,5</sup> Since this early work, theoretical and experimental<sup>21-27</sup> research on the maser amplifier and oscillator has indicated that these devices could have great practical values in areas ranging from RF heating of fusion plasmas to new radar systems. For applications such as plasma heating, high efficiency is of prime importance.

The operation of the electron cyclotron maser oscillator can be viewed qualitatively as the exchange of energy from a system of nonlinear oscillators (electrons) to the fields of a cavity. We describe briefly the steady state operation of a maser cavity in which electrons are entering and radiation is emitted at a uniform rate. The electrons enter the cavity, gyrating about an applied longitudinal magnetic field. Since the electron cyclotron frequency is energy dependent, because of relativistic effects, these electrons can be viewed as nonlinear (or nonisochronous) oscillators. The electron cyclotron frequency decreases as the electron kinetic energy increases. We choose the initial conditions to be such that the cyclotron frequency of the entering electrons is slightly lower than the fixed Doppler shifted frequency of the cavity field. As the initially randomly phased electrons drift through the cavity some of them lose, while others will

gain, kinetic energy, depending on the initial value of their Larmor phase with respect to the electric field. The electrons which gain energy undergo a decrease in rotational frequency, causing them to move further from resonance with the cavity fields. Those electrons which lose kinetic energy, on the other hand, get closer to resonance with the fields and lose energy faster and for a longer time. Thus it is possible to have a net decrease in electron kinetic energy for a time after the electrons enter the cavity. If the electrons were to remain within the cavity they would eventually begin to gain back a portion of the net kinetic energy lost. However, in designing a practical cavity, the transit time of the electrons is made equal to the time it takes the average electron kinetic energy to reach a minimum. In the steady state the  $Q$  of the cavity is chosen such that the radiated power just balances the rate of kinetic energy lost by the electrons. For a comprehensive treatment of the nonlinear and linear theory of the cyclotron maser amplifier see Ref. (17). A number of excellent review papers<sup>8, 28-30</sup> are available which discuss the physical mechanism and applications of the maser in more detail.

Theoretical and experimental progress has been made in improving the maser oscillator efficiency by contouring the walls and thus the fields of the cavity. Experimental efficiencies of  $\sim 40\%$  at wavelengths of  $\sim 9$  mm and continuous powers of  $\sim 20$  kW have been achieved.<sup>(21)</sup>

It is the purpose of this paper to analyze the nonlinear particle dynamics in the cyclotron maser and address the problem of efficiency enhancement. We show that by appropriately contouring the applied magnetic field or the cavity electric field as a function of axial position, the beam electrons can be prebunched in phase, resulting in a significant increase in efficiency over the already high intrinsic value. Although we analyze a maser oscillator configuration, our method of enhancing the efficiency is applicable to a maser amplifier with minor changes.

## II. ANALYSIS

## a. Maser Cavity Model

We shall consider a steady state maser cavity oscillator with the geometry shown in Fig. 1. The electron beam drifts in the  $z$ -direction and gyrates about the applied axial magnetic field  $B_0 \hat{e}_z$ . The beam consists of a thin current sheet, uniform in the  $y$ -direction, with the guiding centers of the electrons initially uniformly distributed on the  $x = 0$  plane. For a sufficiently low-current beam, we may take the cavity fields to be given by the unperturbed normal modes of the cavity. For definiteness we assume that the beam drives a single  $TE_{0,m,n}$  mode. The only non-vanishing field components for this mode are

$$E_y(x, z, t) = \sum_{m,n} E_{m,n} \cos(\omega_{m,n} t + \phi_{m,n}) \sin(K_n z) \sin(k_m(a - x))$$

$$B_x(x, z, t) = \sum_{m,n} \frac{c K_n}{\omega_{m,n}} E_{m,n} \sin(\omega_{m,n} t + \phi_{m,n}) \cos(K_n z) \sin(k_m(a - x)),$$

$$B_z(x, z, t) = \sum_{m,n} \frac{c k_m}{\omega_{m,n}} E_{m,n} \sin(\omega_{m,n} t + \phi_{m,n}) \sin(K_n z) \cos(k_m(a - x)), \quad (1a,b,c)$$

where  $E_{m,n}$  and  $\phi_{m,n}$  is the mode amplitude and phase,  $k_m = m\pi/2a$ ,  $K_n = n\pi/L$ ,  $\omega_{m,n} = c\sqrt{k_m^2 + K_n^2}$  and  $m,n = 1, 2, 3, \dots$ . For strong coupling, the electric field must be maximum at the beam location, i.e.  $m$  odd, and have a frequency close to the electron cyclotron frequency.

## b. Particle Dynamics

The particles enter the cavity at  $z = 0$ , randomly phased, with the same axial velocity  $v_{0z} = \beta_{0z}c$  and the same transverse velocity  $v_{0\perp} = \beta_{0\perp}c$ . In order to obtain tractable nonlinear orbit equations we make a number of simplifying assumptions, all of which are physically well founded. We assume that the transverse wavelength of the cavity mode,  $2\pi/k_m$ , is large compared to the electron Larmor radius as well as the excursions of the particle guiding centers in

the  $x$ -direction, hence  $|k_m x| \ll 1$ ,  $\sin(k_m(a - x)) \approx \sin(k_m a)$  and  $\cos(k_m(a - x)) \approx xk_m \sin(k_m a)$  for  $m$  odd. The particle velocities are considered to be mildly relativistic, *i.e.*,  $(\dot{z}/c)^2$ ,  $(\dot{x}/c)^2$  and  $(\dot{y}/c)^2 \ll 1$ . Finally we assume that the cavity is long, *i.e.*,  $L \gg 2a$ , and that the cavity field amplitude is small compared to the applied magnetic field, *i.e.*,  $|E_{m,n}/B_0| \ll 1$ .

For a single  $TE$  cavity mode the orbit equations, in the absence of self-fields, take the approximate form

$$\begin{aligned} \frac{d}{dt}(\gamma \dot{x}) &\approx -\Omega_o \dot{y} \\ \frac{d}{dt}(\gamma \dot{y}) &\approx \Omega_o \dot{x} - \frac{|e|}{m_o} E \sin(ka) \sin(Kz) \cos(\omega t + \phi) \\ \frac{d(\gamma \dot{z})}{dt} &\approx 0 \end{aligned} \quad (2a,b,c)$$

where  $\gamma = (1 - (\dot{x}^2 + \dot{y}^2 + \dot{z}^2)/c^2)^{-1/2} \geq 1$ ,  $\Omega_o = |e|B_0/m_o c$ . The subscripts on  $E_{m,n}$ ,  $k_m$ ,  $K_n$ ,  $\omega_{m,n}$  and  $\phi_{m,n}$  have been dropped. In obtaining Eqs. (2), some higher order terms have been neglected, these terms are typically smaller than the dominant terms by the factor  $(\dot{z}/c)(cK/\omega)(xk) \ll 1$ .

From Eqs. (2a) and (2c) we find that the canonical momenta in the  $x$  direction as well as the axial velocity of the particles in the cavity are approximately conserved, *i.e.*,  $\gamma \dot{x} + \Omega_o \dot{y} = 0$  and  $\dot{z} = v_{oz}$ . Making use of these two approximate constants, Eq. (2b) can be put into the form

$$\begin{aligned} \ddot{y} + \Omega_o^2(1 - \beta_{oz}^2 - \Omega_o^2 y^2/c^2 - \dot{y}^2/c^2)y \\ = -\frac{|e|}{m_o} E \sin(ka) \sin(Kv_{oz}(t - t_0)) \cos(\omega t + \phi), \end{aligned} \quad (3)$$

where  $t_0$  is the entry time of the particle into the cavity and we have used the approximation  $\gamma \approx 1 + (\beta_{oz}^2 + \Omega_o^2 y^2/c^2 + \dot{y}^2/c^2)/2$ . The phase bunching process in the cyclotron maser

occurs on a time scale which is slow compared to the cavity wave period or electron cyclotron period. Since  $Kv_{oz} \ll \omega \approx \Omega_o$ , we see that the solution to Eq. (3) can be written in the form

$$y = r(t)\sin(\omega t + \theta(t)) \quad (4)$$

where  $r$  and  $\theta$  vary slowly in time, i.e.,  $|r/r|, \dot{\theta} \ll \omega$ . Substituting Eq. (4) into (3) and using the approximations  $\Omega_o^2 y^2 + \dot{y}^2 \approx \omega^2 y^2$  and

$$\Omega_o^2(1 - \beta_{oz}^2 - \omega^2 r^2/c^2) - \omega^2 \approx -2\omega[\omega - \Omega_o[1 - (\beta_{oz}^2 + \omega^2 r^2/c^2)/2]],$$

we find that  $r$  and  $\theta$  satisfy the following equations:

$$\dot{r} = -\epsilon c \sin(Kv_{oz}t)\cos(\theta - \phi),$$

$$\dot{\theta} = \Omega_o/\gamma(r) - \omega + \frac{\epsilon c}{r} \sin(Kv_{oz}t)\sin(\theta - \phi), \quad (5a, b)$$

where  $\gamma(r) = 1 + 1/2(\beta_{oz}^2 + \omega^2 r^2/c^2) \geq 1$  and  $\epsilon \equiv (E/2B_0)\sin(ka) \ll 1$ . In deriving Eqs. (5) we have neglected small terms in  $\ddot{r}$ ,  $\ddot{\theta}$ ,  $\dot{r}\dot{\theta}$  and  $\dot{\theta}^2$ . Note that the particle time of entry,  $t_0$ , can be arbitrarily set equal to zero without loss of generality.

Since  $\Omega_o \approx \omega$ , the term  $\omega r/c$  can be identified as the magnitude of the transverse particle velocity. The kinetic energy of a particle in the cavity is  $E = (\gamma - 1)m_e c^2$  and is a function of  $r$  only. The evolution of  $r$ , given by the simultaneous solutions of Eqs. (5), gives the particle energy as a function of time (axial position) in the cavity. The nonisochronous nature of the maser process is evidenced by the fact that the electron cyclotron frequency (the first term on the RHS of Eq. (5b)) is energy dependent because of the relativistic term  $\omega^2 r^2/c^2$ . The energy dependent cyclotron frequency is responsible for the phase bunching of the particle ensemble, which is initially distributed randomly in  $\theta$ .

### c. Forward or Backward Wave Coupling

The standing wave associated with a cavity mode is the superposition of a forward and a backward propagating wave. We may further simplify the description of the nonlinear particle

dynamics contained in Eqs. (5) by noting that under certain conditions the beam particles will predominantly couple to either the forward or backward wave. This will permit us to derive a useful constant of the motion for analyzing the nonlinear dynamics of the particles. To see this we define the variable  $\xi_{\pm} = \theta \pm Kv_{oz}t$  and note that for small cavity field levels, i.e.,  $\epsilon \rightarrow 0$ ,  $\xi_{\pm}$  is appropriately given by

$$\xi_{\pm} \approx \Delta\omega_{\pm}t + \theta_0$$

where  $\Delta\omega_{\pm} = \omega - \Omega_0/\gamma(r_0) \mp Kv_{oz}$ . Interaction with the forward wave implies  $|\Delta\omega_+| \gg |\Delta\omega_-| \approx 0$  while for the backward wave resonance we would have  $|\Delta\omega_+| \gg |\Delta\omega_-| \approx 0$ . If, however,  $|\Delta\omega_+| \approx |\Delta\omega_-|$ , both waves couple to the beam about equally and the overall interaction is weak, resulting in low efficiency. It is, therefore, desirable and possible, by properly choosing the system parameters, to have one of the wave interactions dominate over the other. If this is done the nonlinear coupled equations in (5a,b) can be put into the form

$$\begin{aligned} \dot{r} &= \mp \frac{\epsilon c}{2} \cos \xi_{\pm} \\ \dot{\xi}_{\pm} &= \Omega_0/\gamma(r) - \omega \pm Kv_{oz} \pm \frac{\epsilon c}{2r} \sin \xi_{\pm} \end{aligned} \quad (6a,b)$$

where without loss of generality,  $\phi$  has been set equal to  $3\pi/2$  in Eqs. (6) and the upper (lower) sign corresponds to forward (backward) wave resonance. These equations are identical in form to those describing the particle orbits in a cavity field that is uniform in  $z$ . For definiteness we will consider only the forward wave resonance case (upper sign); this implies that  $\omega > \Omega_0/\gamma$ . With obvious changes in parameter definitions our results apply directly to the backward wave resonance case. Dropping the subscript on  $\xi_{\pm}$  we get

$$\begin{aligned} \dot{r} &= \frac{-\epsilon c}{2} \cos \xi, \\ \dot{\xi} &= \Omega_0/\gamma(r) - \omega + \frac{\epsilon c}{2r} \sin \xi. \end{aligned} \quad (7a,b)$$

where  $\tilde{\omega} = \omega - Kv_{0z}$ . This system of equations is equivalent to that obtained from the well known Duffing equation on a slow time scale.<sup>11</sup> The nonlinear orbits defined by Eqs. (7) can be shown to have the following constant of motion

$$C(r, \xi) = \frac{1}{\Omega_0 \omega} (\tilde{\omega} - \Omega_0 / \gamma(r))^2 - \epsilon \frac{\omega r}{c} \sin \xi \quad (8)$$

Typical curves in  $(r, \xi)$  space are shown in Fig. (2) for various values of  $C$ . In general, particles may lie on open or closed (trapped) orbits.

Particles starting on a particular constant-of-motion curve remain on this curve. The rate at which the particles move along the  $C$ -curves is governed by the solutions of the orbit equations in (7). We assume no interaction among the particles themselves (*i.e.*, we neglect space-charge effects). Thus we may represent the beam by an ensemble of a small number of particles, typically 32. Numerically solving Eqs. (7), for such an initial ensemble of particles, the distribution of particles for various times (or axial positions within the cavity) is shown in Fig. (3). The particles enter the cavity uniformly distributed in  $\xi$  over an interval of  $2\pi$  radians, all with the same initial value of transverse velocity, *i.e.*,  $r = r_0$ , see Fig. (3a). As time progresses, the particles move along their respective  $C$ -curves. In the linear regime (Fig. 3b) a significant amount of spreading in  $r$  along with a small degree of bunching in  $\xi$  has developed. As the particles begin to bunch in phase angle  $\xi$  (Fig. 3c) most of them are contained within the energy loss regime  $-\pi/2 < \xi < \pi/2$  and considerable spreading in  $r$  has occurred. The particles are distributed over a wide range of  $C$ -curves, with two ensuing consequences. First, as the particles lose energy they move out of the energy loss region,  $-\pi/2 < \xi < \pi/2$ . Secondly not all the particles reach their minimum energy at the same time. Figure (3d) shows the particle ensemble in the saturated state where the particles are deeply trapped and the average

transverse kinetic energy is at a minimum. If permitted, the particle ensemble would continue to rotate and regain the lost kinetic energy.

The efficiency of energy extraction from the particles is defined as

$$\eta(t) = N_p^{-1} \sum_{i=1}^{N_p} (\gamma(r_i(t)) - \gamma(r_o)) / (\gamma(r_o) - 1) \quad (9)$$

where

$$\gamma(r_i(t)) = \gamma(r_o) + \omega^2 c^{-2} (r_i^2(t) - r_o^2) / 2$$

(c.f. below Eqs. (5) ),  $r_o = r_i(t=0)$  and  $r_i(t)$  is the Larmor radius of the  $i$ th particle which entered the cavity with phase angle  $0 < \xi_i < 2\pi$ , and  $N_p$  is the number of particles in the ensemble. In order to have a standard comparison between various sets of parameters we shall henceforth consider the transverse efficiency, defined by  $\eta_{\perp}(t) = \eta(t)(\gamma(r_o) - 1) / (\omega r_o / c)^2$ . Thus,  $\eta_{\perp}(t)$  is the efficiency associated with the transverse beam kinetic energy and is independent of  $v_{0z}$ . The transverse energy efficiency is given in Fig. (4) as a function of time for the parameters of Fig. (3). The net energy extracted reaches a maximum at  $t = t_s = 165/\bar{\omega}$ ; the length of the actual cavity would be  $L = v_{0z} t_s$ . Figure (5) shows the peak transverse efficiency as a function of  $\epsilon$ , for  $v_{0\perp}/c = 0.3$  and various values of the frequency mismatch parameter  $\Delta\omega = \bar{\omega} - \Omega_o / \gamma(r_o)$ . From these curves we see that the maximum transverse efficiency is approximately 40%. This maximum intrinsic efficiency of approximately 40% is characteristic for the range of  $v_{0\perp}/c$  of interest in the maser. We note that in our treatment the steady state value of  $\epsilon$  is taken to be compatible with the  $Q$  of the cavity.

### III. ENHANCEMENT OF MASER EFFICIENCY

A qualitative appreciation of the nonlinear particle dynamics can be gained from an examination of the C-curves and phase space trajectories, depicted in Figs. 2 and 3. We note that

since the particles are not all on the same *C*-curves they reach their minimum energies at different times. Furthermore the minimum energy varies widely over the ensemble of particles. We are thus led to the conclusion that the efficiency can be dramatically increased by first prebunching the particles in phase space. The resulting "macro-particle" can then be placed on a set of *C*-curves for which virtually 100% of the transverse kinetic energy is extracted.

To see in detail how this can be accomplished we must examine the basic orbit equations in (7). We consider the linear regime of these equations by expanding *r* and  $\xi$  in powers of the normalized electric field  $\epsilon$ . For  $\epsilon$  sufficiently small we can write  $r = r^{(0)} + \epsilon r^{(1)}$  and  $\xi = \xi^{(0)} + \epsilon \xi^{(1)}$  where  $r^{(0)}$ ,  $r^{(1)}$ ,  $\xi^{(0)}$ ,  $\xi^{(1)}$  are independent of  $\epsilon$ . The solution of (7) in the linear regime is  $r^{(0)} = r_0$ ,  $\xi^{(0)} = \xi_0 - \Delta\omega t$  and

$$r^{(1)} = \frac{c}{2\Delta\omega} (\sin(\xi_0 - \Delta\omega t) - \sin \xi_0),$$

$$\xi^{(1)} = \frac{c}{2\Delta\omega r_0} \left[ \left( 1 - \frac{\Omega_0}{\Delta\omega} \frac{\omega^2 r_0^2}{c^2} \right) (\cos(\xi_0 - \Delta\omega t) - \cos \xi_0) + \Omega_0 t \frac{\omega^2 r_0^2}{c^2} \sin \xi_0 \right] \quad (10a,b)$$

where  $|\epsilon r^{(1)}| \ll r^{(0)}$ , and  $|\epsilon \xi^{(1)}| \ll \xi^{(0)}$ . The standard deviations of *r* and  $\xi$  are measures of the spreads of the particle ensemble in phase space and are defined respectively as  $\sigma_r = (\langle r^2 \rangle - \langle r \rangle^2)^{1/2}$  and  $\sigma_\xi = (\langle \xi^2 \rangle - \langle \xi \rangle^2)^{1/2}$  where  $\langle \dots \rangle = (2\pi)^{-1} \int_0^{2\pi} d\xi_0 (\dots)$ . In the linear regime we find

$$\sigma_r = \alpha (1 - \cos \Delta\omega t)^{1/2} r_0,$$

$$\sigma_\xi = \left[ \frac{\pi^2}{3} - 2\alpha \left\{ \frac{\omega^2 r_0^2}{c^2} \Omega_0 t + \left( 1 - \frac{\Omega_0}{\Delta\omega} \frac{\omega^2 r_0^2}{c^2} \right) \sin \Delta\omega t \right\} \right]^{1/2}. \quad (11a,b)$$

where  $\alpha = \epsilon c / (2r_0 \Delta\omega)$  will be denoted as the "bunching parameter." The mean values of *r* and  $\xi$  are  $\langle r \rangle = r_0$  and  $\langle \xi \rangle = \pi - \Delta\omega t$ . These linearized equations are valid if  $\alpha \ll 1$ . From Eqs. (11) we note that  $\sigma_r$  is bounded while  $\sigma_\xi$  decreases secularly in time. Therefore, if  $\alpha \ll 1$ , the particle distribution will bunch into a macro-particle with phase space dimensions of

$$\Delta r \approx \sqrt{2}\alpha r_0.$$

$$\Delta\xi \approx (\pi^2/3 - 2\alpha(\omega r_0/c)^2 \Omega_0 t)^{1/2}, \quad (12a,b)$$

Note that the expression for  $\Delta\xi$  is invalid for times such that  $\Omega_0 t \geq \pi^2(6\alpha(\omega r_0/c)^2)^{-1}$ . The point to be made by Eqs. (12) is that  $\Delta r$  is bounded and  $\Delta\xi$  initially decreases with time if  $\alpha$  is sufficiently small. The formation and dimensions of the macro-particle in phase space is schematically depicted in Fig. 6. As shown in Fig. 6, all the particles lie on open trajectories and the formation of the macro-particle takes place over many cyclotron periods, with only a small degree of spreading in  $r$ .

We can tailor the bunching parameter such as to achieve minimum  $\sigma_\xi$  when the macro-particle enters the energy loss region  $\cos\xi > 0$ . When the macro-particle enters this region the bunching parameter can be increased such as to deform the trajectories of the macro-particle onto a bundle of closed C-curves for which virtually all the transverse kinetic energy can be extracted. The change in  $\alpha$  should occur over an axial distance roughly equal to  $v_0/\Delta\omega$ , in order to ensure that the macro particle remains in the energy loss region. The bunching parameter can be changed as a function of axial position in the cavity by (i) varying  $K$  as a function of  $z$  (for example by axially contouring the cavity wall radius) and/or (ii) varying the external magnetic field,  $B_0$ , as a function of  $z$ . From the definition of the bunching parameter,  $\alpha = \epsilon c/(2r_0\Delta\omega)$ , we see that these methods can lead to a large fractional change in  $\alpha$  with only modest changes in either  $K$  or  $B_0$ . As an illustration of contouring  $\alpha$  by method (ii) we choose the magnetic field variation depicted in Fig. 7. The initial parameters are  $\epsilon = 0.004$ ,  $\beta_{01} = 0.3$  and  $\Delta\omega/\bar{\omega} = 0.08$ . The initial value of the bunching parameter is  $\alpha = 0.077$  (see Fig. 7). The particles reach their maximum degree of bunching at  $\bar{\omega}t \approx 225$ , just before entering the energy loss region, see Fig. 8. At this point the frequency mismatch is decreased gradually to the value  $\Delta\omega/\bar{\omega} = 0.02$  at  $\bar{\omega}t = 260$ . This is accomplished by increasing the external magnetic field

by about 6%. The bunching parameter has the final value  $\alpha = 0.31$  at the end of the transition region and the macro particle is now on a trapped orbit. The maximum transverse kinetic energy loss occurs at  $\bar{\omega}t = 400$  resulting in a transverse efficiency of  $\eta_{\perp} = 75\%$ . The transverse efficiency as a function of time is shown in Fig. 9. As shown in Fig. 5, without contouring the applied magnetic field the transverse efficiency is 36% for these parameters with constant  $\Delta\omega/\bar{\omega} = 0.02$ .

#### IV. CONCLUSION

We have shown that dramatic increases in the efficiency of the maser oscillator can be achieved by appropriately tailoring either the applied axial magnetic or the cavity field (cavity wall radius). It should be noted that this approach can be directly applied, with appropriate modifications, to a maser amplifier device. We have illustrated in detail an example for which the applied magnetic field is tailored. The requisite field variations are quite modest and technologically straightforward. No attempt has been made to obtain an optimum field profile, as it is our purpose to present the general principle of efficiency enhancement and show that dramatic increases can be readily achieved. As a standard of comparison we have considered only the transverse efficiency,  $\eta_{\perp}$ , which is independent of  $v_{0z}$ . In principle, the energy associated with the longitudinal motion may be largely recovered by using depressed collectors, so that the overall system efficiency may be made to approach  $\eta_{\perp}$ .

#### ACKNOWLEDGEMENTS

We thank Drs. K. R. Chu, V. L. Granatstein and A. T. Drobot for stimulating discussions.

SPRANGLE AND SMITH

REFERENCES

1. R.Q. Twiss, *Australian J. Phys.* **11**, 564 (1958).
2. J. Schneider, *Phys Rev. Lett.* **2**, 504 (1959).
3. A.V. Gaponov, *Izv. Vyssh. Uchebn. Zaved., Radiofizi*, **2**, 450 (2959).
4. R.H. Pantell, *Proc. IRE*, **47**, 1146 (1959).
5. J.L. Hirshfield and J.M. Wachtel, *Phys. Rev. Lett.* **12**, 533 (1964).
6. G. Bekefi, Jay L. Hirshfield and Sanborn C. Brown, *Phys. Rev.* **122**, 1037 (1961).
7. J. L. Hirshfield, I.B. Bernstein and J.M. Wachtel, *J. Quantum Electronics*, Vol. QE-1, 237 (1965).
8. A.V. Gaponov, M. I. Petelin, and V. K. Yulpatov, *Radiophys. Quantum Electron.*, **10**, No. 9-10, 794-813 (1967).
9. A. V. Gaponov, and Y.K. Yulpatov, *Radio Eng. Electron. Phys.* **12**, No. 4, 582-586 (1967).
10. G.N. Rapoport, A. K. Nemak, and V.A. Zhurakhovskiy, *Radio Eng. Electron. Phys.* **12**, No. 4, 587-595 (1967).
11. Matthew Borenstein and Willis E. Lamb, Jr. *Phys. Rev. A*, **5**, 1298 (1972).
12. V.L. Bratman, M.A. Moiseev, M.I. Petelin and R.E. Erm, *Radiophys. Quantum Electron.*, **16**, 474 (1973).

NRL MEMORANDUM REPORT 3983

13. V.L. Bratman and A.E. Tokarev, Radiophys Quantum Electron. 17, No. 8, 932-935 (1974).
14. P. Sprangle and Wallace M. Manheimer Phys. of Fluids, 18, 224 (1975).
15. Edward Ott and Wallace M. Manheimer, IEEE Trans on Plasma Sci Vol. PS-3, No. 1 (1975).
16. P. Sprangle, J. Applied Phys. 47, 2935 (1976).
17. P. Sprangle and A.T. Drobot, IEEE Trans. on Microwave Theory and Techniques Vol. MTT-25, No. 6, 528 (June 1977).
18. K.R. Chu, Phys. of Fluids 21, (Dec. 1978).
19. Hwan-sup Uhm, R.C. Davidson and K.R. Chu, Phys of Fluids 21, 1866 (1978).
20. R.L. Schriever and C.C. Johnson, Proc. IEEE 54, 2029 (1966).
21. D.V. Kisel', G.S. Korablev, V.G. Navel'yev, M.I. Petelin and Sh. E. Tsimring, Radio Engineering and Electronic Physics, 19, 95 (1974).
22. N.I. Zaytsev, T.B. Pankratova, M.I. Petelin, and V.A. Flyagin, Radio Eng. Electron. Phys 19, 103-106 (1974).
23. M. Friedman, D.A. Hammer, W.M. Manheimer and P. Sprangle, Phys. Rev. Letters 31, 752 (1973).
24. V.L. Granatstein, P. Sprangle, M. Herndon, R.K. Parker and S.P. Schlesinger, Journal of Applied Physics 46, 3800 (1975)

SPRANGLE AND SMITH

25. V.L. Granatstein, M. Herndon, P. Sprangle, Y. Carmel and J.A. Nation, *Plasma Physics* **17**, 23 (1975).
26. V.L. Granatstein, P. Sprangle, M. Herndon and R.K. Parker, *Journal of Applied Physics* **46**, 2021 (1975).
27. Jory, H., S. Hegji, J. Shively, and R. Symons, *Microwave J.* **21**, 30 (1978).
28. V.A. Flyagin, A.V. Gaponov, M.I. Petelin and V.K. Yulpatov, *IEEE Trans. Macrowave Theory Tech.* **MTT-25**, 514 (1977).
29. J.L. Hirshfield and V.L. Granatstein, *IEEE Trans. Microwave Theory Tech.* **25**, 522 (1977).
30. A.A. Andronov, V.A. Flyagin, A.V. Gaponov, A.L. Gol'denberg, M.I. Petelin, V.G. Usov, and V.K. Yulpatov, report for Submillimeter Waves, Institute of Applied Physics, Gorky Academy of Sciences of the USSR (1978).

NRL MEMORANDUM REPORT 3983

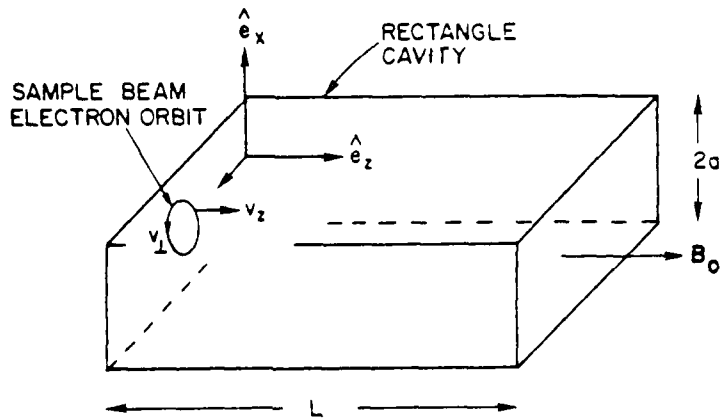


Fig. 1 — Model of the electron cyclotron maser cavity oscillator

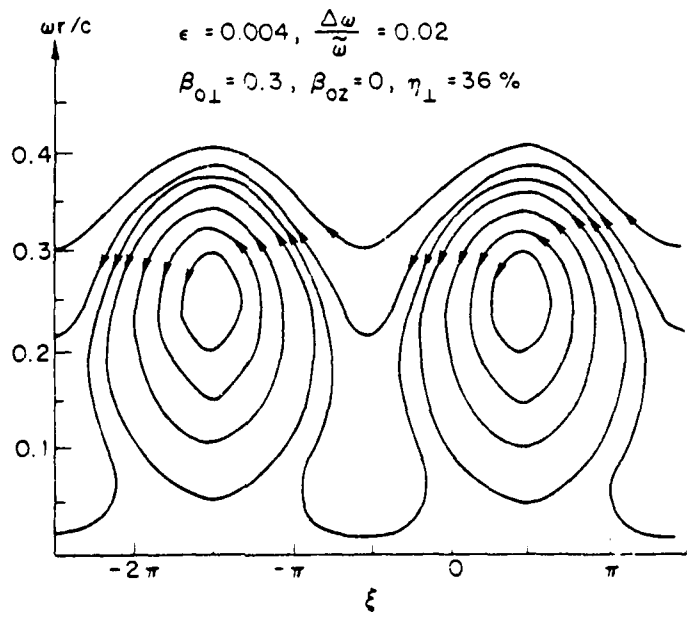


Fig. 2 — Typical phase space curves of the constant of motion  $C(r, \xi)$

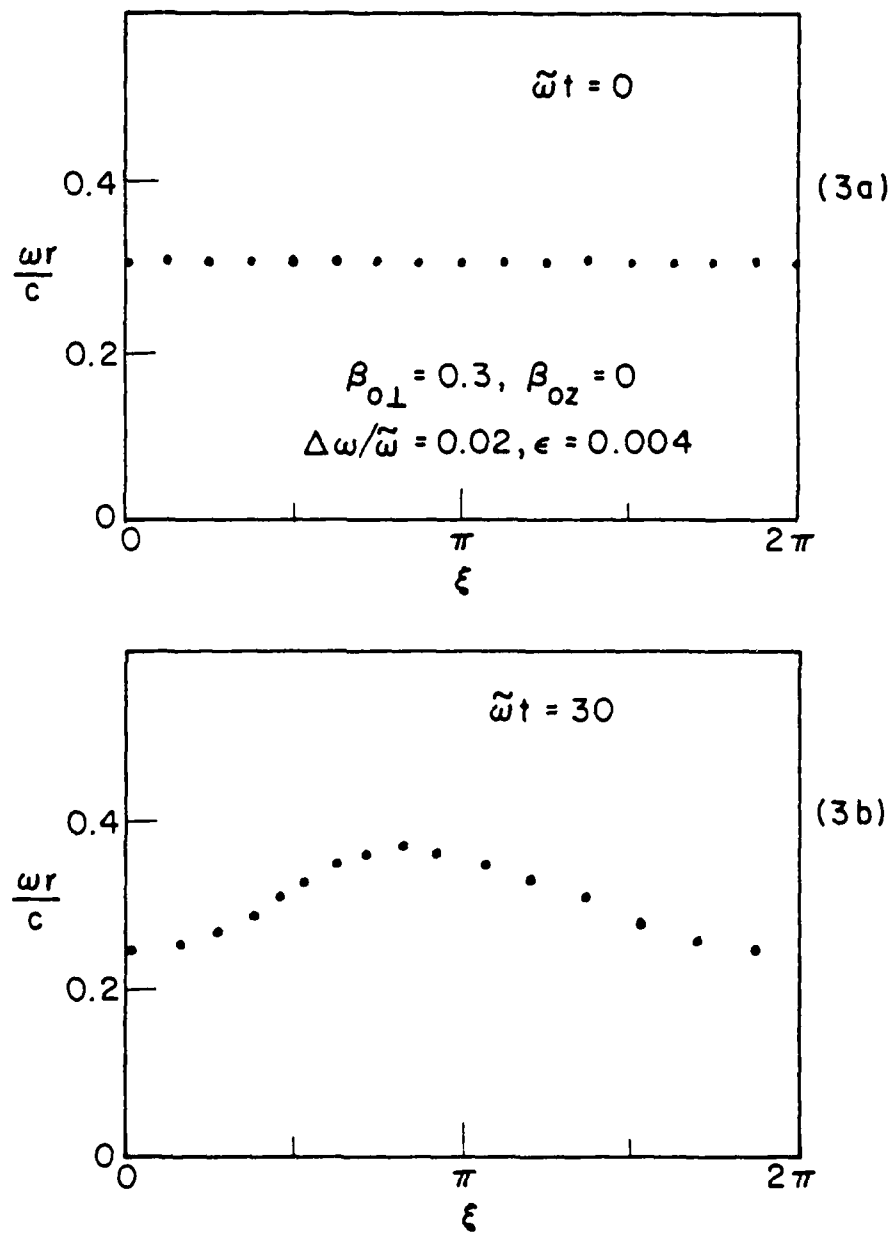


Fig. 3 — Phase space evolution of an ensemble of 16 particles in the fields of the cavity. The system parameters are the same as those used for Fig. (2) a) initial particle distribution. b) linear regime of interaction. c) phase bunching regime. d) energy extraction regime (Saturation).

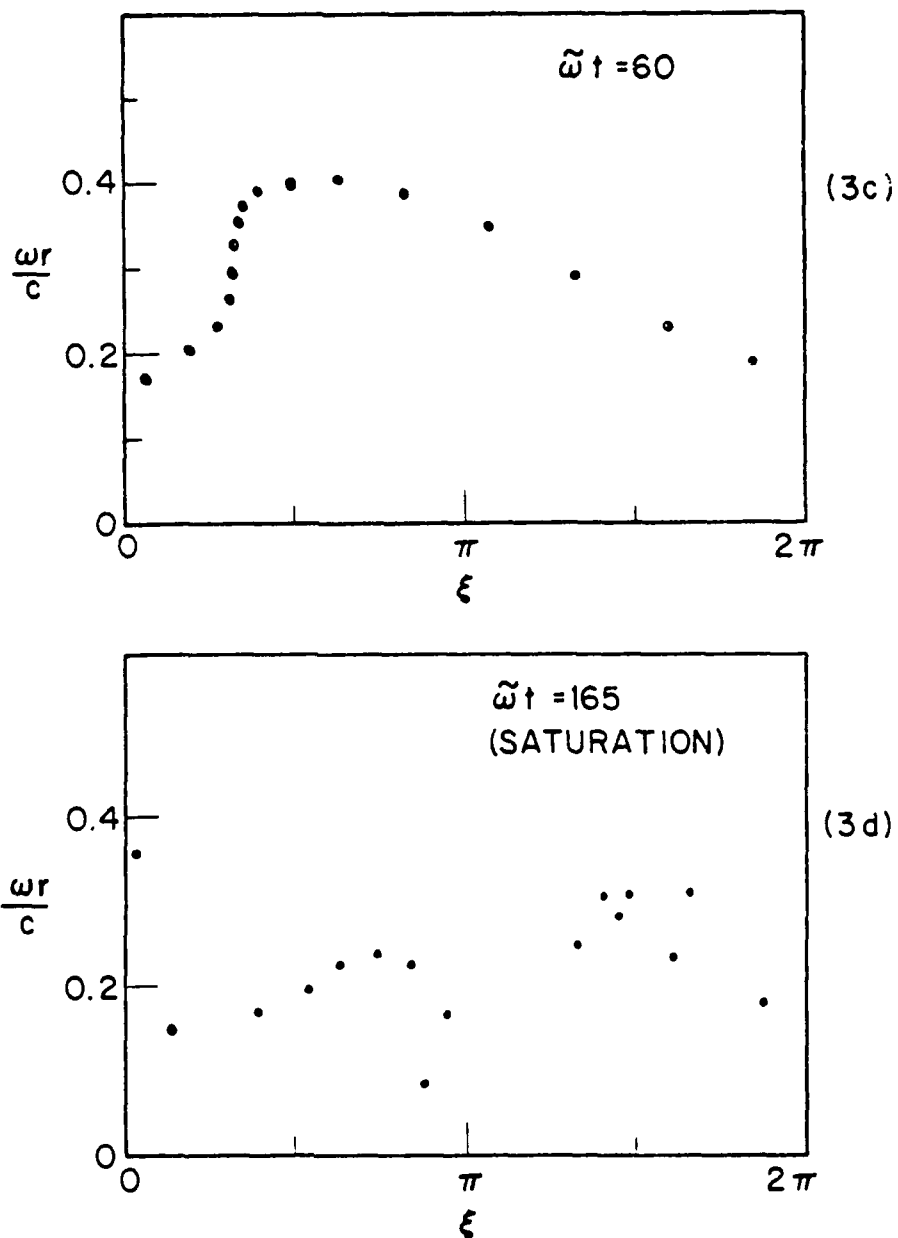


Fig. 3 (Continued) — Phase space evolution of an ensemble of 16 particles in the fields of the cavity. The system parameters are the same as those used for Fig. (2). a) initial particle distribution b) linear regime of interaction c) phase bunching regime d) energy extraction regime (Saturation)

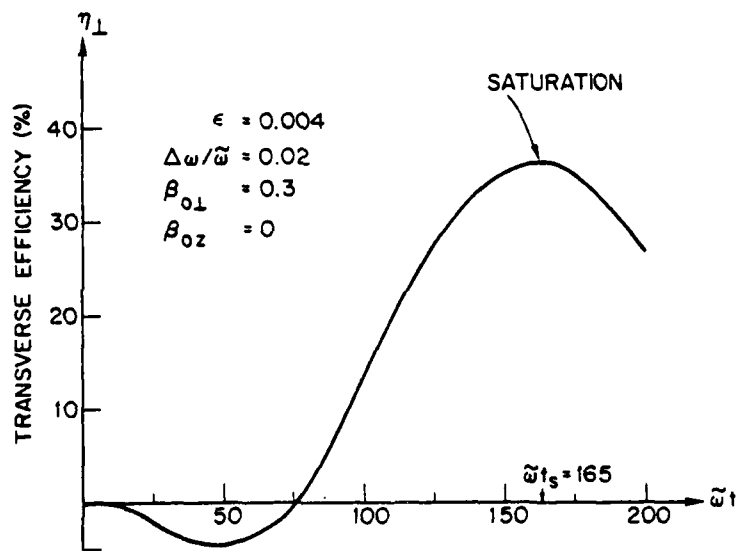


Fig. 4 — Transverse energy efficiency as a function of time  
(axial position within cavity)

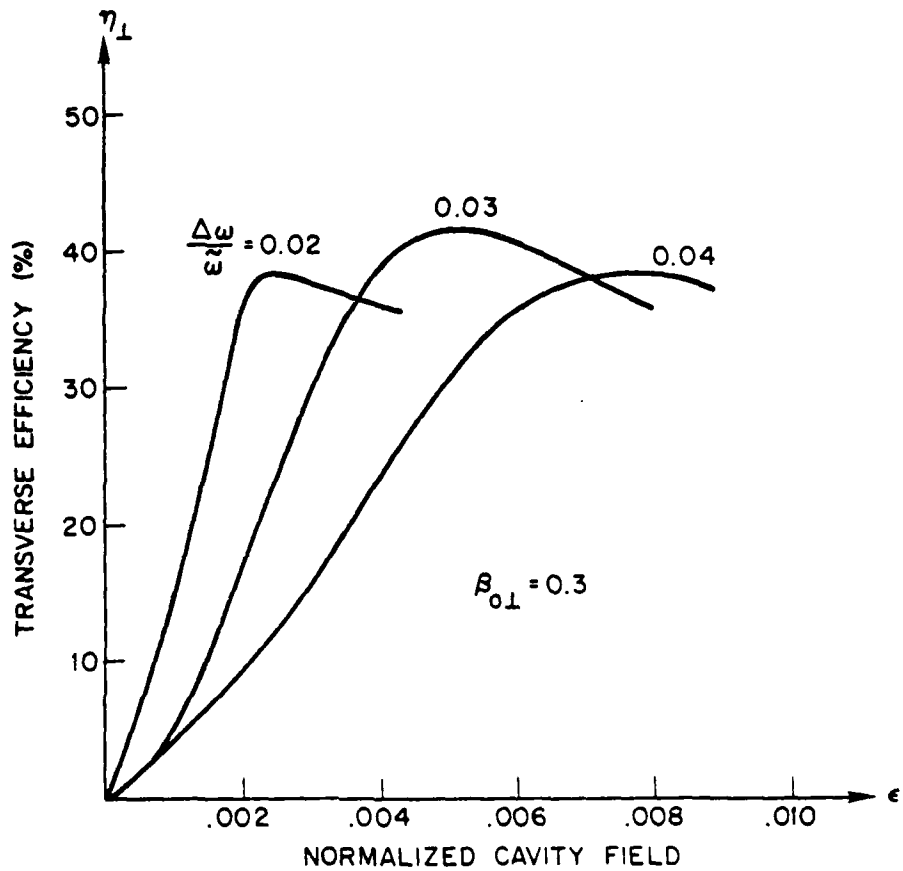


Fig. 5 — Saturation efficiencies as a function of the normalized cavity field,  $\epsilon$ , for various values of  $\Delta\omega/\omega$ . These results are for uniform  $B_0$  and  $K$ .

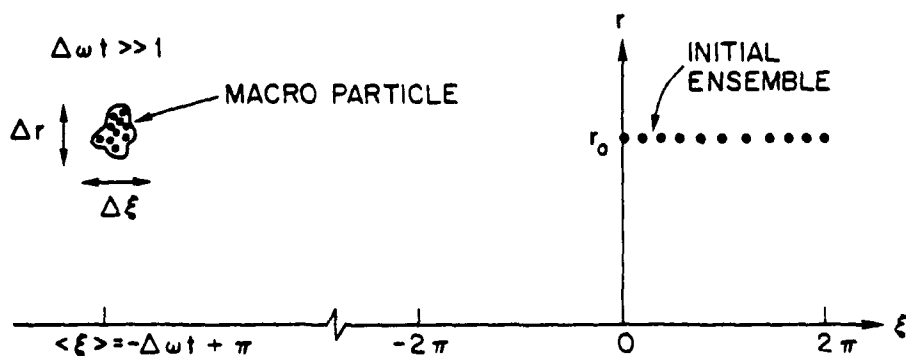


Fig. 6 — Schematic of phase space evolution illustrating the formation of a macro-particle when the bunching parameter,  $\alpha$ , is much less than unity

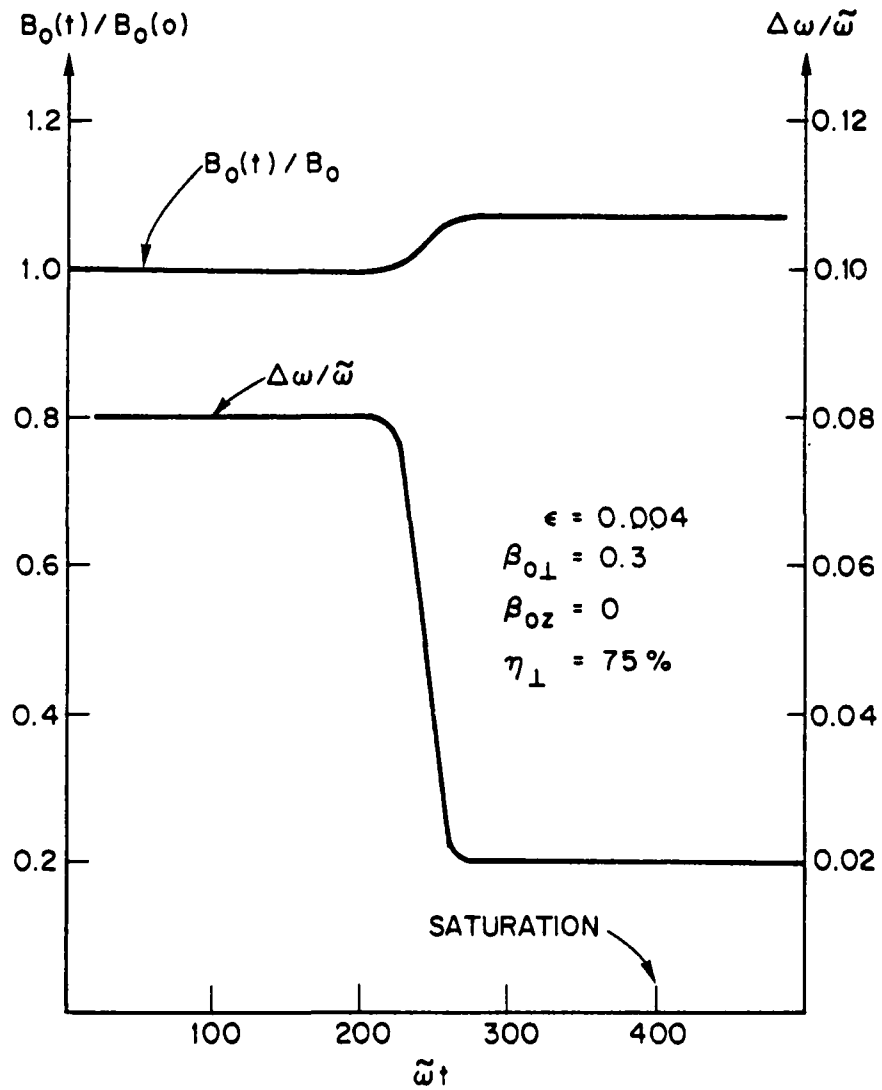


Fig. 7 — Contoured magnetic field profile as a function of time (axial position in the cavity) in the forward wave interaction approximation. The final parameters correspond to the uniform field system of the previous example (Fig. 2-4).

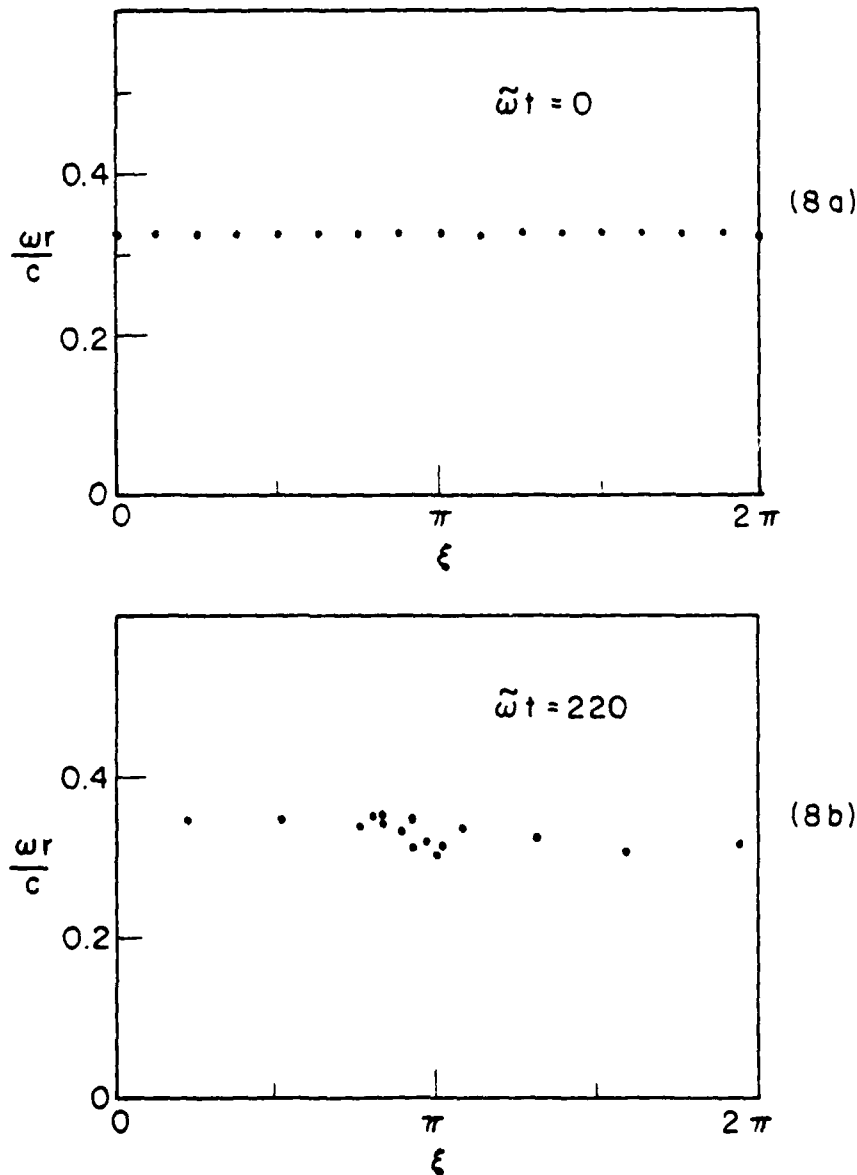


Fig. 8 — Phase space evolution for the field profile shown in Fig. 7 a) initial distribution of particles; b) formation of macro-particle just before entering contoured applied magnetic field region; c) the macro-particle after it leaves the contoured applied magnetic field region. d) particle distribution at saturation.

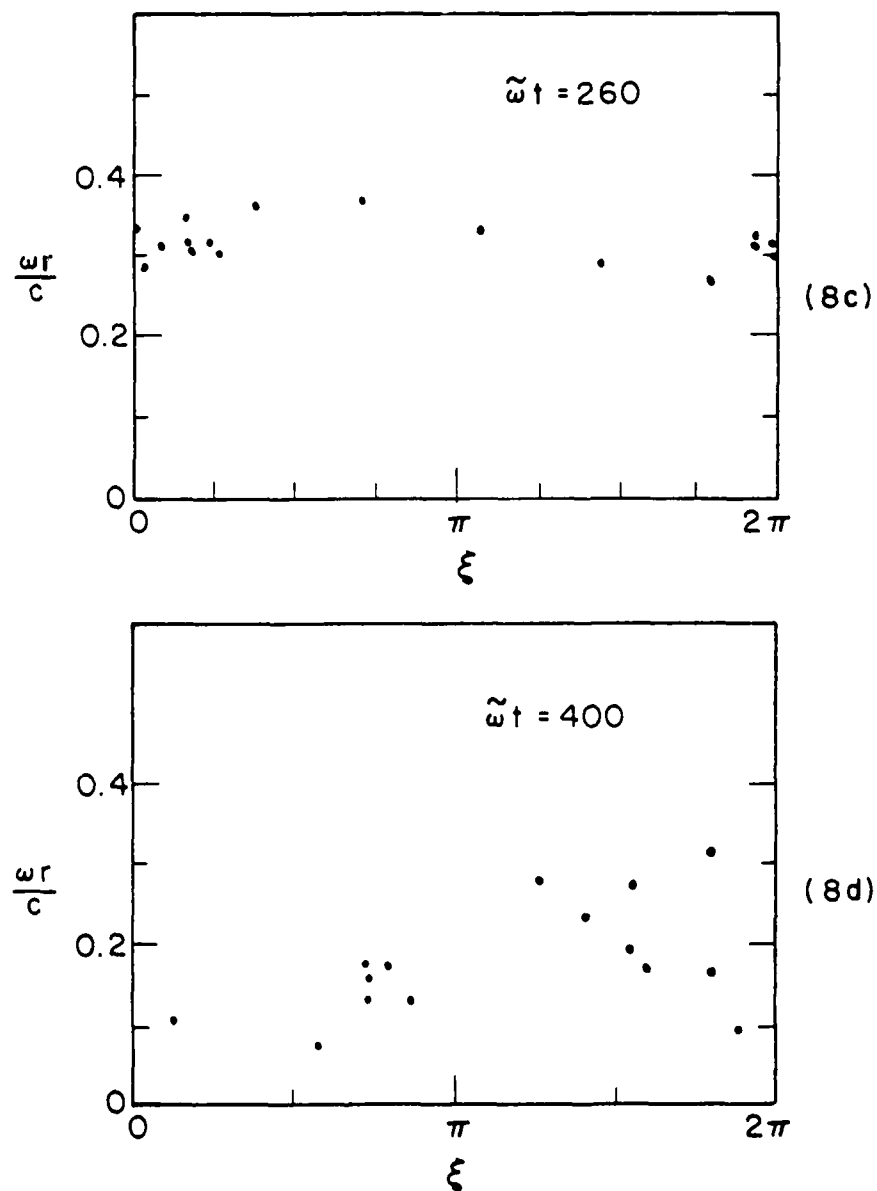


Fig. 8 (Continued) — Phase space evolution for the field profile shown in Fig. 7: a) initial distribution of particles; b) formation of macro-particle just before entering contoured applied magnetic field region; c) the macro-particle after it leaves the contoured applied magnetic field region; d) particle distribution at saturation.

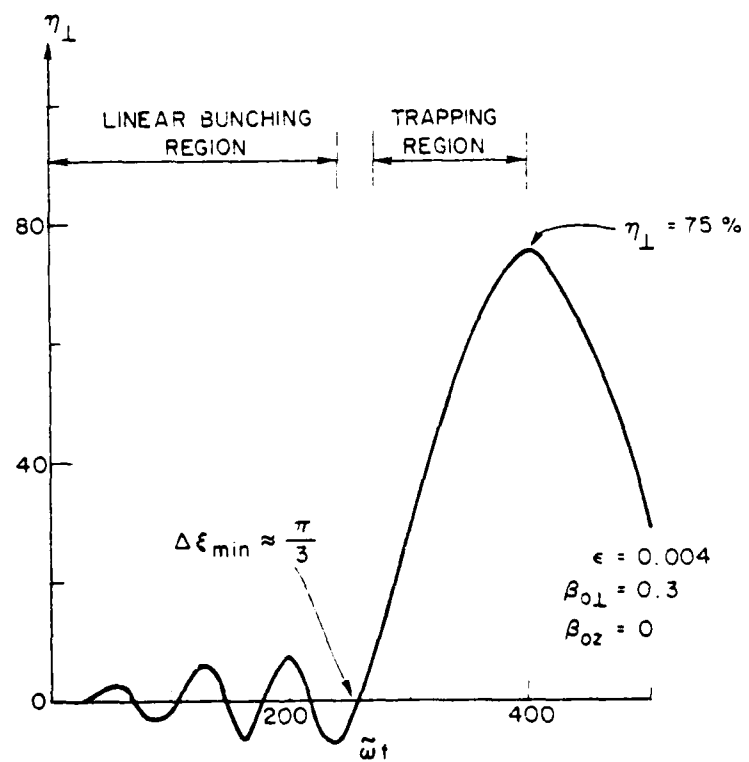


Fig. 9 — Transverse efficiency as a function of time (axial position in the cavity) for the system shown in Figs. (7) and (8)

